HOKKAIDO UNIVERSITY

Title	Investigation on the susceptibility of transgenic mice and rat neuronal cell line Rn33B that express equine major histocompatibility class 1 to equine herpesvirus-1
Author(s)	港, 江利奈
Degree Grantor	北海道大学
Degree Name	博士(獣医学)
Dissertation Number	甲第14116号
Issue Date	2020-03-25
DOI	https://doi.org/10.14943/doctoral.k14116
Doc URL	https://hdl.handle.net/2115/78511
Type	doctoral thesis
File Information	Erina_MINATO.pdf

Hokkaido University Collection of Scholarly and Academic Papers : HUSCAP

Investigation on the susceptibility of transgenic mice and rat neuronal cell line Rn33B that express equine major histocompatibility class 1 to equine herpesvirus-1

（ウマ主要組織適合遺伝子複合体クラス 1 遺伝子導入マウスおよびラット由来神経細胞株 Rn33B におけるウマヘルペスウイルス 1 型感受性の検討）

Erina Minato

Table of Contents

Table of contents……01

Abbreviations…….…....02

General Introduction……...…….…….……03

Chapter 1

Exogenous expression of equine major histocompatibility class 1 in mice increases susceptibility to equine herpesvirus-1 pulmonary infection

Introduction……...……...06

Material and Methods……...……...…….07

Results……...……...….13

Discussion…….……...15

Figures……..18

Summary……...……...….25

Chapter 2

Susceptibility of rat immortalized neuronal cell line Rn33B expressing equine major histocompatibility class 1 to equine herpesvirus-1 infection is differentiation-dependent

Introduction……...……...….27

Materials and Methods…….29

Results……...……...….34

Discussion…….……...….39

Figures……...……42

Summary……...……...….50

Conclusion…….…….……...….51

Acknowledge…….…….……...….53

References…….…….…….55

Summary in Japanese…….…….....63

Abbreviations

APC:	allophycocyanin
β2m:	β2-microgloburin
CNS:	central nerve system
DAB:	diaminobenzidine
EHV-1:	equine herpesvirus-1
EBMECs:	Equine brain microvascular endothelial cells
GFP:	green fluorescent protein
HE:	hematoxylin and eosin
HRP:	horseradish peroxidase
HSV-1:	herpes simplex virus-1
IFN:	interferon
IHC:	immunohistochemistry
ISGs:	interferon stimulated genes
MEMECs:	Murine brain microvascular endothelial cells
MHC class 1:	Major histocompatibility class 1
NGF:	Nerve growth factor
PBMC:	Peripheral blood mononuclear cell
PBS:	phosphate-buffered saline
PCR:	polymerase chain reaction
PFU:	plaque forming units
p.i.:	post-infection
poly(dA:dT):	poly(deoxyadenylic-deoxythymidylic)
RK13 cells:	rabbit kidney 13 cells
Rn33B-A68B2M:	Rn33B cells expressing equine MHC class 1
RT-PCR:	Reverse transcription-polymerase chain reaction
SAB:	streptavidin-biotin
SDS-PAGE:	sodium dodecyl sulfate-polyacrylamide gel electrophoresis
Tg:	transgenic
WT:	wild-type

General Introduction

Equine herpesvirus-1 (EHV-1) is an alphaherpesvirus of the family *Herpesviridae*. EHV-1 causes respiratory disease, abortion, and myeloencephalopathy, which results in severe economic loss in horse industries. Outbreaks of EHV-1 have been reported around the world (1–6). There are no effective treatments. Modified live and inactivated vaccines are used to prevent EHV-1 infection, but cases of myeloencephalopathy in highly vaccinated adult horses have been reported (3,7–9).

In horses, following oronasal transmission, EHV-1 infection occurs in respiratory epithelial cells and local lymph nodes (7,10). This results in a leukocyte-associated viremia, followed by the infection of endothelial cells in the pregnant uterus and central nervous system (CNS) (9). The pathologic consequences of endothelial infection in the uterus and CNS are vasculitis, thrombosis and secondary ischemia that cause abortion (11) and neurological signs (12), respectively. EHV-1 establishes latent infection in T lymphocytes (13) and/or in trigeminal ganglia (14).

Large amounts of experimental data have been generated from experimental infections using horses. Peripheral blood mononuclear cells (PBMCs) collected from horses infected with EHV-1 is used to identify the subpopulation of viremic PBMC in the early infection (15). Experiments using EHV-1-infected primary equine monocytes elucidate EHV-1 pathogenesis in those cells (16,17). Horses are also used to evaluate a vaccine candidate (18,19). However, experiments using horses are labor-intensive. In addition, there are difficulties in obtaining large numbers of horses for experiments. Therefore, small animals have been used to develop the models for EHV-1 infection.

Unlike other alphaherpesviruses that show strong neurotropism, neuronal

infection is not observed in EHV-1 myeloencephalopathy. The mechanism underlying the resistance of neurons to EHV-1 infection is unclear, due to the lack of a suitable neuronal cell culture model. Murine neuronal cell lines, such as PC-12 and Neuro2A, have been used as experimental models of infection with herpes simplex virus-1 (HSV-1) (20–22). However, murine neuronal cell lines are not suitable as a model for EHV-1 infection *in vitro*, because the majority of murine cell lines are resistant to EHV-1 infection.

Recently, an equine major histocompatibility class 1 (equine MHC class 1) heavy chain *A68* gene has been reported as a functional entry receptor for EHV-1 (23,24). MHC class 1 molecule has the three extracellular domains (α1, α2, α3) and is polygenic and pleomorphic. EHV-1 utilizes equine MHC class 1 molecules with the hydrophobic amino acids residue at position 173 in α2 domain (24). Because mouse MHC class 1 molecule has the hydrophilic amino acids at position 173, mouse MHC class 1 molecule is unlikely to work as a receptor for entry into murine cells (24). Mouse NIH3T3 cells, which express mouse MHC class 1 molecules (haplotype H2q) (25,26) on their surface, are not susceptible to EHV-1 infection. However, exogenous expression of equine MHC class1 genes in NIH3T3 cells confers susceptibility to EHV-1 infection (23).

The present study was performed to establish convenient models for EHV-1 experimental infection *in vivo* and *in vitro*. In chapter 1, transgenic mice expressing equine MHC class 1 were generated to confirm that exogenous expression of equine MHC class 1 rendered mice more susceptible to EHV-1. In chapter 2, rat neuronal cell line lentivirally transduced with equine MHC class 1 was established to demonstrate that the susceptibility of cells to EHV-1 was different between undifferentiated status and neuronally-differentiated status.

Chapter 1

Exogenous expression of equine major histocompatibility class 1 in mice increases susceptibility to equine herpesvirus-1 pulmonary infection

Introduction

Equine herpesvirus-1 (EHV-1) causes respiratory disease, abortion, and myeloencephalopathy. In horses, EHV-1 infection occurs in respiratory epithelial cells, mononuclear cells and endothelial cells. Especially, the pathologic consequences of endothelial infection in the uterus and CNS are vasculitis, thrombosis and secondary ischemia that cause abortion (11) and neurological signs (12), respectively.

Experimental infections using horses are labor-intensive. Mice have also been used as models for EHV-1 infection. EHV-1-infected mice are reported to show pneumonia, viremia (27), and abortion (28). However, neither viral replication in the endothelial cells nor the subsequent formation of CNS lesion has been reported in the murine model. Equine brain microvascular endothelial cells (EBMECs) are susceptible to EHV-1 infection, whereas their murine counterparts (MEMECs) are EHV-1 resistant, reflecting the inability of the virus to enter mouse cells (29).

Equine major histocompatibility class 1 (equine MHC class 1), a functional entry receptor of EHV-1, has been reported to render murine cells susceptible to EHV-1 infection (23,24). In the current study, transgenic mice (Tg mice) expressing equine MHC class 1 was generated to verify its ability to act as an entry receptor for EHV-1 *in vivo* and make mice more susceptible to EHV-1 infection. After inoculation with EHV-1, the histopathological changes in Tg mice were compared with those in their wild-type (WT) littermates to evaluate the effect of equine MHC class 1 expression on EHV-1 pathogenicity.

Materials and methods

Virus

The EHV-1 strain Ab4 (30) was kindly provided by Dr. Hideto Fukushi (Gifu University, Gifu, Japan). Stock viruses were cultured in rabbit kidney (RK13) cells, and titrated by plaque formation assays on RK13 cells.

Plasmid

The plasmid vector pCXSN was generated as previously described (23). The plasmid pCAGGS-MCS(KS), which was kindly provided by Dr. Naomi Ohnishi (Japanese Foundation for Cancer Research, Tokyo, Japan), was generated from pCAGGS (31) by replacing the cloning sites with *Kpn*I, *Xho*I, *Eco*RI, and *Sac*I endonuclease recognition sequences.

Tg mice

DNA fragments of equine MHC class 1 heavy chain *A68* (GenBank/EMBL/DDBJ entry AB525079) excised from pCXSN-A68-HA (23) were cloned into the *Xho*I-*Hind*III site of a pSP73 vector (Promega, Wisconsin, USA) to generate vector pSP-A68. The construction of pSP-V5 68 was done by the insertion of a V5 epitope tag following the putative signal alignment of *A68* into the pSP-A68 vector using inverse polymerase chain reaction (PCR). The region of DNA containing the equine *β2-microglobulin (β2m)* was amplified by PCR from plasmid pCXSN-equine β2m (23), and cloned into the *Hind*III-*Eco*RI site of pSP-V5 68 (pSP-V68-B2M). To induce bicistronic expression of the equine MHC class 1 heavy chain *A68* and *equine β2m* on

the cell surface, 2A oligopeptide (ATNFSLLKQAGDVEENPGP) (32) was inserted between the C terminus of A68 and the N terminus of β2M in pSP-V68-B2M using inverse PCR (pSP-V68-2A-B2M). The V68-2A-B2M fragment was then excised as an *Xho*I-*Eco*RI fragment, and cloned into vector pCAGGS-MCS(KS) to generate the vector pCAGGS-V68-2A-B2M. The equine MHC class 1 heavy chain *A68* with *equine β2m* excised from pCAGGS-V68-2A-B2M as a *Sna*BI-*Hind*III fragment was used as a transgene (Fig. 1). The transgene was microinjected into fertilized eggs of Slc:BDF1 mice (Japan SLC,Inc., Shizuoka, Japan). The transgenic founders carrying the *A68* gene were backcrossed with BALB/cAJcl (CLEA Japan, Inc., Tokyo, Japan). The mouse line designated BALB/cAJcl;BDF1-Tg (CAG-Eq-MHC-I-B2M) 30LCP/A68 was used in this study as Tg mice.

Genotyping of Tg mice

The founder and its progeny were genotyped by PCR. Mouse tail-derived DNA was used as template. PCR was performed with 2 × Quick Taq HS DyeMix (TOYOBO, Osaka, Japan), 0.2 μM each of the primers, and 200 ng of DNA. Details of the PCR primers used for the amplification are shown in Table 1. For the amplification of the *A68* gene, primers A68-B2M-F1 and PCAGGS-REV were used; for amplification of mouse actin, primers mouse actin F and mouse actin R were used. The PCR cycling profile was 94 °C for 2 min for denaturation, followed by 35 sequential cycles of 94 °C for 30 s, 63 °C for 30 s, and 72 °C for 1 min. The PCR products were electrophoretically analyzed on 1.5% agarose gels.

Reverse transcription-polymerase chain reaction (RT-PCR)

The liver, spleen, kidneys, and lung of Tg mice were collected. Total RNA was extracted using the TRIZOL reagent (Thermo Fisher Scientific, Massachusetts, USA). The RNA samples were treated with DNase I, Amplification Grade (Thermo Fisher Scientific) to digest contaminating DNA. Synthesis of complementary DNA (cDNA) was carried out using the SuperScript^{TM} III First-Strand Synthesis System (Thermo Fisher Scientific). PCR was performed with 0.2 mM dNTP, 10 × PCR buffer, 1.5 mM $MgCl_2$, 1.25 units of HotStarTaq DNA Polymerase (Qiagen, Hilden, Germany), 0.3 μM of each primer, and 1 μl of cDNA in a total volume of 12.5 μl. The PCR primers used for the amplification were the same as those used in genotyping of Tg mice. The PCR cycling profile was 95 °C for 15 min for initial denaturation; followed by 40 sequential cycles of 94 °C for 30 s, 63 °C for 1 min, and 72 °C for 1 min; and final extension at 72 °C for 10 min. The PCR products were electrophoretically analyzed on 1.5% agarose gels.

Western Blot

The liver, spleen, lung, and brain of Tg mice or WT mice were collected. The tissues were lysed in lysis buffer (10 mM Tris-HCl, pH 7.5; 150 mM $NaCl_2$; 5 mM EDTA; 10% glycerol; and 1% Triton X-100) supplemented with complete protease inhibitor cocktail (MERCK, Darmstadt, Germany). Lysed proteins were homogenized and sonicated. Following sodium dodecyl sulfate polyacrylamide gel electrophoresis (SDS-PAGE), proteins were transferred onto Immobilon-P transfer membranes (Merck Millipore, Massachusetts, USA), and labeled with anti-V5 antibody (1/5000 dilution, Thermo Fisher Scientific), or anti-actin antibody clone C4 (1/5000 dilution, Merck Millipore).

Immunofluorescence staining

The lungs of Tg mice or WT mice were collected, and the tissues were fixed in 4% paraformaldehyde/phosphate-buffered saline (PBS), pH 7. The tissues were paraffin-embedded, and sections were prepared using standard methods. Indirect immunofluorescence staining was performed using Tyramide SuperBoost kits with Alexa Fluor Tyramides (Thermo Fisher Scientific). Briefly, the sections were deparaffinized, heated with 0.01 M citric acid buffer (pH 6.0) using a microwave for antigen retrieval, treated with 0.3% hydrogen peroxide in methanol, and blocked with 10% normal rabbit serum. A goat anti-V5-tag polyclonal antibody (1/500 dilution, ab95038; Abcam, Cambridge, England) was added, and the sections were incubated overnight at 4 °C. The sections were then washed with PBS, and incubated with donkey anti-goat horseradish peroxidase (HRP)-conjugated IgG (1/500 dilution, Santa Cruz Biotechnology, Texas, USA) for 20 min at room temperature. After further washing with PBS, the sections were incubated with Alexa Fluor 488 Tyramide Reagent for 10 min at room temperature. Nuclei were stained with Hoechst 33258 (MERCK). As a negative control, sections were stained without primary antibody. The fluorescent-stained sections were examined using an LSM 700 confocal microscope (Zeiss, Oberkochen, Germany).

Experimental infection

Heterozygous Tg mice and WT littermate mice were used at six weeks of age. Seven Tg mice and three WT mice were anesthetized with isoflurane, and intranasally inoculated with 2×10^6 plaque forming units (PFU) of EHV-1 Ab4. All animal experiments were authorized by the Institutional Animal Care and Use Committee of the Graduate School of Veterinary Medicine, Hokkaido University (approval number: 13-

0092), and all experiments were performed according to the guidelines of this committee.

Histopathology and Immunohistochemistry

The mice inoculated with EHV-1 were euthanized and necropsied at 3 days post-inoculation (d p.i.). The liver, spleen, kidneys, heart, lung, and brain were collected. All organs were fixed with 4% paraformaldehyde/PBS. The tissues were paraffin-embedded, sectioned at 2 to 4 μm, and stained with hematoxylin and eosin (HE). To calculate the number of necrotic bronchiolar epithelial cells in the lungs, the total number of bronchiolar epithelial cells showing necrotic morphology in each section and the total area of the sections was measured using a CellSens Dimension microscope (Olympus, Tokyo, Japan). The number of necrotic cells was divided by the total area of each section. The mean number of necrotic cells in the bronchioles of Tg mice was compared with those of WT mice using the Welch two-sample *t*-test.

Indirect immunohistochemistry staining was carried out using the labeled streptavidin-biotin (SAB) technique (Histofine SAB-PO Kit, Nichirei, Japan). Briefly, the sections were deparaffinized, heated with 0.01 M citric acid buffer (pH 6.0) using a microwave for antigen retrieval, treated with 0.3% hydrogen peroxide in methanol, and blocked with 10% normal rabbit serum. Goat anti-equine rhinopneumonitis virus/equine herpesvirus type 1 polyclonal antiserum (1/5000 dilution, VMRD, Washington, USA) or polyclonal rabbit anti-human CD3 antibody (ready-to-use, Agilent, California, USA) was added, and the sections were incubated overnight at 4 ºC. The sections were then washed with PBS, and incubated with a secondary antibody labeled with biotin for 20 min at room temperature. After additional washing with PBS, the sections were incubated with peroxidase-conjugated streptavidin for 10 min at room temperature. The bound

peroxidase was detected with 3,3'-diaminobenzidine (DAB). The sections were counterstained with hematoxylin. As a negative control, sections were stained without primary antibody.

To calculate the number of cells in the lungs that were positive for viral antigen, the total number of EHV-1-positive cells were counted in each section of the tissue and the total area of the sections was measured using a CellSens Dimension microscope. The number of positive cells was divided by the total area of each section. The mean number of EHV-1-positive cells in the lungs of Tg mice was compared with the number in the lungs of WT mice using the Welch two-sample *t*-test.

To calculate the number of T cells in the lung, CD3-positive cells were counted in each tissue section using ImageJ (33). The number of positive cells was divided by the total area of each section. The mean number of CD3-positive cells was statistically compared in Tg and WT mice by using the Mann-Whitney U test.

Results

Tg mice expressing equine MHC class 1

Tg mice transduced with equine MHC class 1 were generated as described in the Materials and methods. Because endogenous MHC class 1 was expressed on most somatic cells (34), the CAG promoter, which can induce ubiquitous gene expression, was used (Fig. 1) (31). The expression of equine MHC class 1 heavy chain mRNA and protein was detected in the heterozygous Tg mice, but not in the WT littermate mice (Fig. 2a). The level of equine MHC class 1 protein in the brain was lower than in the liver, spleen, and lung (Fig. 2b). Immunofluorescence staining revealed the expression of equine MHC class 1 on the apical surface of bronchiolar epithelial cells of the Tg, but not of the WT mice (Fig. 3). The expression of equine MHC class 1 was not detected by immunofluorescent staining in the liver, spleen, kidneys, heart, or brain of both of Tg and WT mice.

Experimental infection

Starting at 1d p.i., all EHV-1-inoculated mice, Tg and WT, began to show tachypnea and lethargy with ruffled fur. At 3 d p.i., all mice inoculated with EHV-1 had postmortem lesions of bronchointerstitial pneumonia, with peribronchiolar, and perivascular infiltration of lymphocytes, macrophages, and neutrophils. Necrosis of the bronchiolar epithelial cells were more evident in Tg mice than in WT mice (Figs. 4a, 5a and 6a; $p < 0.05$). Using IHC, EHV-1 was detected in the nucleus and cytoplasm of bronchiolar epithelial cells and macrophages in both groups of mice (Figs. 4b, 4c, 5b, and 5c). More EHV-1-positive cells were found in the lungs of Tg mice than those of WT

mice (Fig. 6b; $p < 0.05$). Furthermore, perivascular edema was much more prominent in the Tg mice; but, virus antigen was not detected in the vascular endothelium (Fig. 4d, 4e, 5d and 5e). Inflammatory cells infiltrating the lung were primarily lymphocytes. The number of CD3-positive cells in the lung did not differ between the two groups of mice (Fig. 6c; $p > 0.05$). Notably, neither histological lesions nor viral antigen were detected in the liver, spleen, kidneys, heart, and brain of Tg or WT mice inoculated with EHV-1.

Discussion

In this study, mice were transduced with equine MHC class 1 molecules, which are known to act as entry receptors for EHV-1 *in vitro*. Western blot analysis showed the expression of equine MHC class 1 proteins in various organs including the lung. After experimental nasal infection with EHV-1, the number of EHV-1-infected cells observed in the lung of Tg mice was higher than in that of WT mice. These results suggest that exogenous expression of equine MHC class 1 increased the susceptibility of mice to EHV-1 infection.

Intranasal infection with EHV-1 in adult BALB/c mice causes bronchiolar epithelial infection as well as pulmonary lesions with intranuclear inclusions and peribronchiolar and perivascular mononuclear cell infiltrates (27). Tg mice developed similar lesions upon EHV-1 intranasal infection. However, infection and necrosis of the bronchiolar epithelium were severer in Tg mice expressing equine MHC class 1 compared to the WT mice. This finding was consistent with the result of immunofluorescent staining that revealed selective expression of equine MHC class 1 expression in the bronchiolar epithelium of Tg mice.

Perivascular edema surrounding pulmonary arteries was a characteristic lesion in both Tg and WT mice, but was more severe in Tg mice than WT mice. Because neither vascular endothelial cells nor vascular smooth muscle cells were positive for viral antigen, the edema may have reflected the severity of adjacent bronchiolar damage.

The role of leukocytes in lung lesion pathogenesis remains unclear. The numbers of CD3-positive cells in the lung were similar in WT and Tg mice, although necrosis and desquamation of bronchiolar epithelial cells were more evident in the Tg mice. Foals

infected with EHV-1 show necrotizing bronchiolitis and infiltration of mononuclear cells (35,36) similar to the lesions of the Tg mice in this study. Smith *et al.* (37) previously reported that mice infected with EHV-1 RacL11 strain developed more severe lung lesions than those infected with attenuated KyA strain. Interestingly, the level of proinflammatory beta chemokines produced in the bronchiolar lavage fluid by RacL11 was higher than that by KyA, despite identical T cell responses and viral loads in the lungs of both strains (37). Therefore, the pathogenesis of the relatively severe lung lesions in EHV-1-infected Tg mice may involve a contribution of the immune response in addition to a direct cytolytic effect of the viral infection.

Immunofluorescence staining of the V5 epitope tag did not show positivity in the liver, spleen, and brain of Tg mouse, although RT-PCR and western blot analyses demonstrated the gene and protein expression of equine MHC class 1 in these organs. It may be that the expression levels of equine MHC class 1 in cell types other than bronchiolar epithelial cells were below the detection limit of the indirect immunofluorescent technique. The CAG promoter used in this study is known to induce high-level gene expression in mammalian cells; but, at times it fails to attain sufficient protein expression levels, depending on the nature of the cargo gene and/or the type of host cell (38). An unknown mechanism was potentially involved in determining the final stationary expression levels of the equine MHC class 1 in the mice.

Neither histological lesions nor viral antigens were detected in the liver, spleen, kidneys, heart and brain of the Tg mouse at 3 days after intranasal inoculation with EHV-1. This was consistent with the paucity of equine MHC class 1 antigen-specific signal obtained in these tissues by immunofluorescent staining. Notably, western blot analysis showed the expression of exogenous protein in all examined organs, albeit at levels below

the detection limit of immunofluorescent staining. Therefore, it will be interesting to investigate the susceptibility of Tg mice to EHV-1 by using alternative routes of virus inoculation.

This study suggests that transgenic expression of equine MHC class 1 is a useful method for increasing the susceptibility of mouse cells to EHV-1 infection *in vivo*. New Tg mice with more widespread overexpression of equine MHC class 1, including additional EHV-1 target cells (e.g. endothelial cells and leukocytes) in addition to bronchiolar epithelial cells may provide a suitable model for the study of EHV-1 pathogenesis.

Figure 1. Construct of the equine MHC class 1 transgene.

V5: gene coding for the V5 epitope tag. *2A*: gene coding for the 2A peptide in which self-cleavage occurs following translation. Arrows: positions of the primers (A68-B2M-F1 and PCAGGS-REV) used for genotyping to detect exogenous expression of equine MHC class 1.

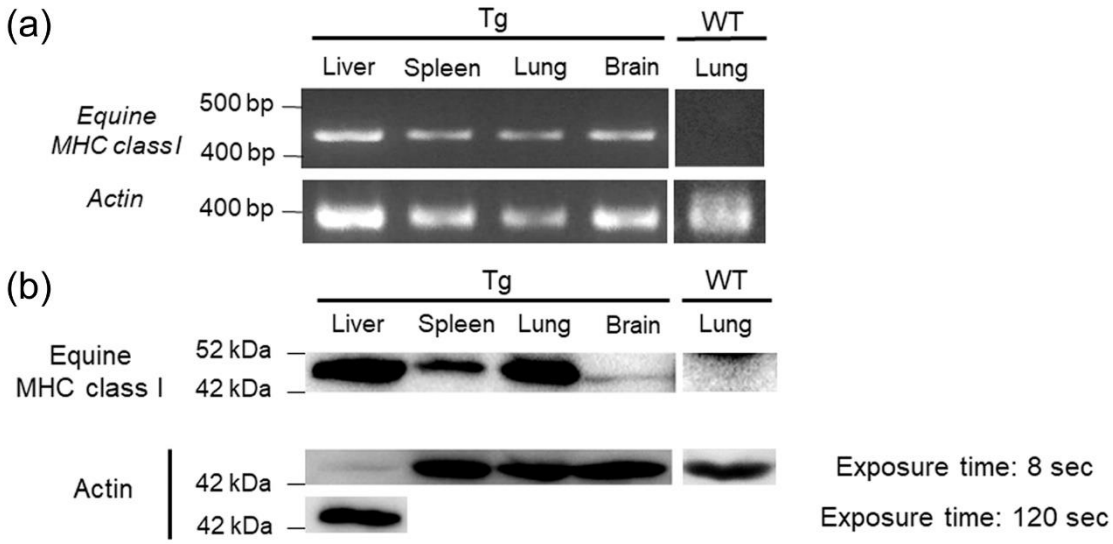

Figure 2. Exogenous expression of equine MHC class 1 in the liver, spleen, lung, and brain of Tg mice.

(a) Expression of *equine MHC class 1* mRNA detected by RT-PCR. *Actin* was used as an internal control. (b) Expression of equine MHC class 1 protein detected by western blot analysis using an anti-V5 antibody. Actin was used as an internal control. A non-specific band with a higher molecular weight was observed in the panel of the lung of WT mouse.

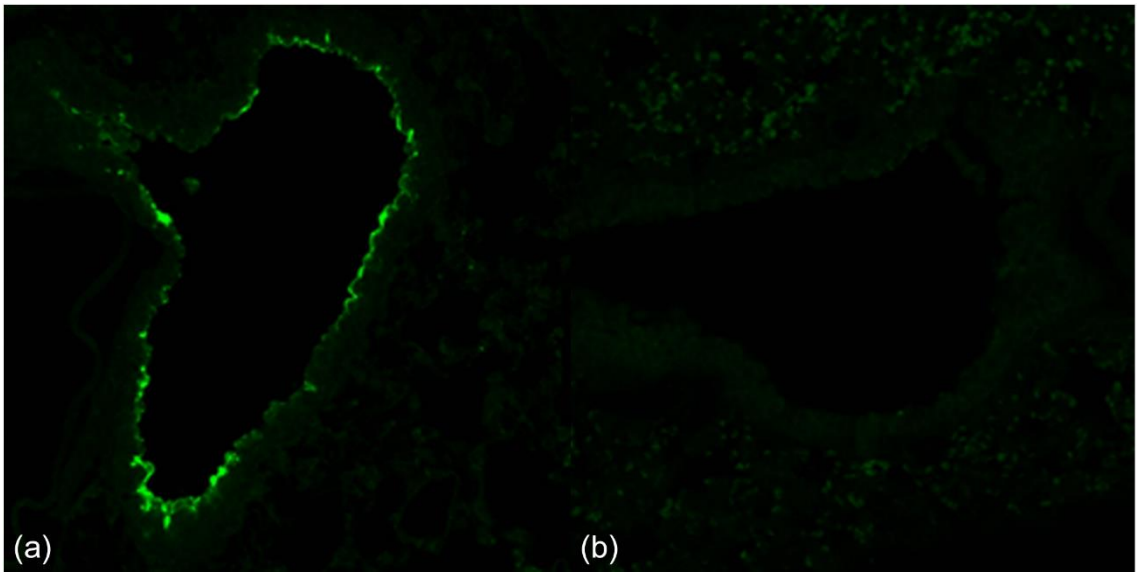

Figure 3. Detection of equine MHC class 1 in the lung by the immunofluorescent staining using an anti-V5 antibody.

Alexa 488 was used as a secondary antibody (green). (a) Bronchiolar epithelial cells of Tg mice were positive for equine MHC class 1. (b) Bronchiolar epithelial cells from WT mice did not express equine MHC class 1.

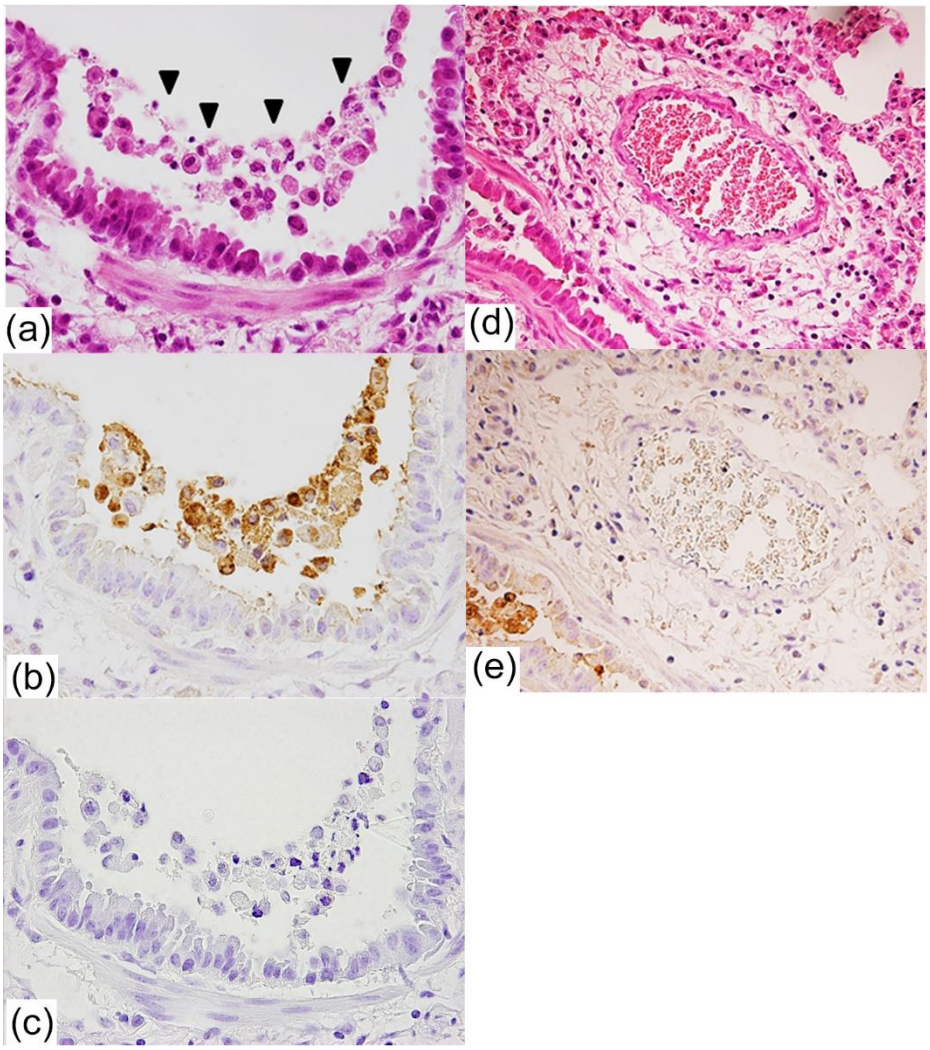

Figure 4. Histopathological changes of the lung in Tg mice infected with EHV-1.

(a) Necrosis and desquamation of bronchiolar epithelial cells. Remaining bronchiolar epithelial cells often showed degeneration. Arrowheads: desquamated epithelial cells. HE. (b, c) IHC for EHV-1 antigens. (b) Positive signals for EHV-1 in most desquamated epithelial cells. (c) Negative control of (b). IHC for the EHV-1 antigen without primary antibody. (d) Perivascular edema. HE. (e) EHV-1 antigen was not detected in vascular endothelial cells. A bronchiole with positive immunolabelling was present at lower left. IHC for EHV-1.

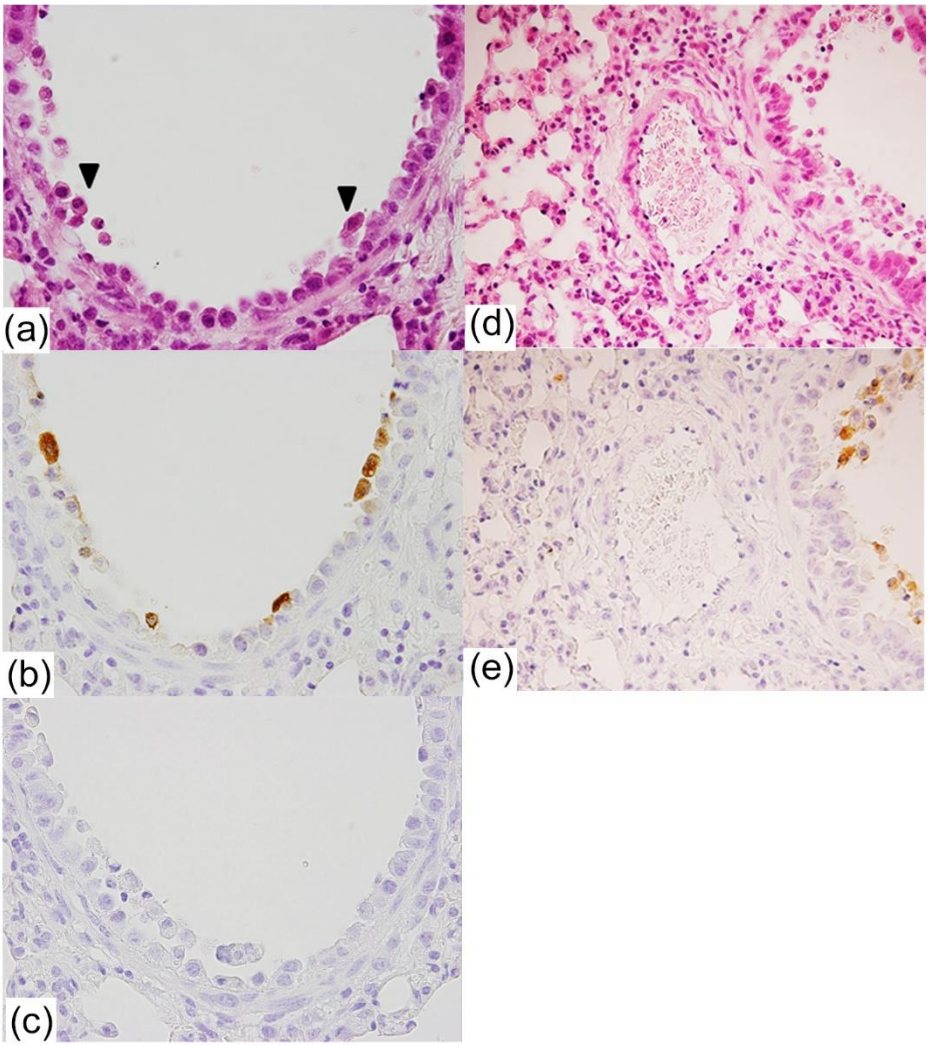

Figure 5. Histopathological changes of the lung in WT mice infected with EHV-1.

(a) Necrosis of few bronchiolar epithelial cells. Arrowheads: desquamated epithelial cells. (b, c) IHC for EHV-1 antigens. (b) Sporadic EHV-1 antigen in the epithelial cells. (c) Negative control of (c). IHC for the EHV-1 antigen without primary antibody. (d) Mild perivascular edema. HE. (e) Vascular endothelial cells were negative for the EHV-1 antigen. A bronchiole with positive immunolabelling is present at right. IHC for EHV-1.

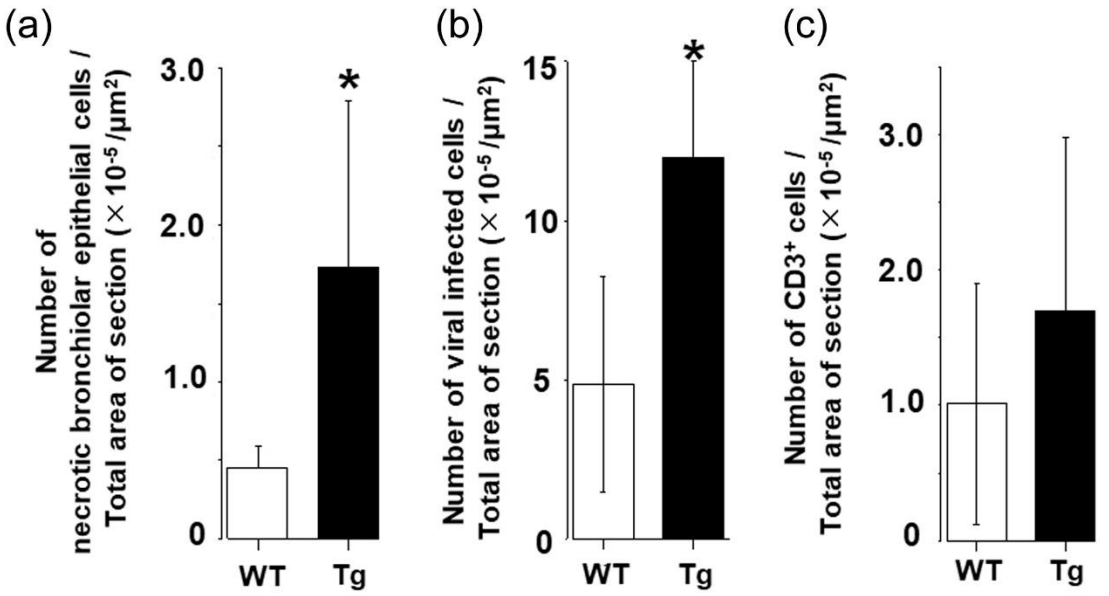

Figure 6. Statistical analysis of Tg and WT mice infected with EHV-1.

(a) Number of necrotic bronchiolar epithelial cells within lungs. Error bars show standard deviations. *$p < 0.05$, Welch two sample *t*-test. (b) Number of EHV-1 antigen-positive cells within lung. Error bars show standard deviations. *$p < 0.05$, Welch two sample *t*-test. (c) Number of CD3-positive cells within lung tissues. Error bars represent standard deviation. $p = 0.3677$, Mann-Whitney U test.

Table 1. Primer sequences

primer name	alignment (5' to 3')	
A68-B2M-F1	AAGAAAACCCCGGGCCTATG	(20 bp)
PCAGGS-REV	TTTGTGAGCCAGGGCATTGG	(20 bp)
mouse actin F	TTCTTTGCAGCTCCTTCGTTGCCG	(24 bp)
mouse actin R	TGGATGGCTACGTACATGGCTGGG	(24 bp)

bp : base pair

Summary

Equine herpesvirus-1 (EHV-1) utilizes equine major histocompatibility complex class 1 (MHC class 1) as an entry receptor. Exogenous expression of equine MHC class 1 genes in murine cell lines confers susceptibility to EHV-1 infection. In order to examine the *in vivo* role of equine MHC class 1 as an entry receptor for EHV-1 *in vivo*, transgenic (Tg) mice expressing equine MHC class 1 were generated under the control of the CAG promoter. Equine MHC class 1 protein was expressed in the liver, spleen, lung, and brain of Tg mice, which was confirmed by western blot. However, equine MHC class 1 antigen was only detected in bronchiolar epithelium and not in other tissues, by using the immunofluorescence method employed in this study. Both Tg and wild-type (WT) mice developed pneumonia 3 days after intranasal infection with EHV-1. The bronchiolar epithelial cells of Tg mice showed severer necrosis, compared with those in WT mice. In addition to this observation, the number of virus antigen-positive cells in the lungs was higher in Tg mice than in WT mice. These results suggest that exogenous expression of equine MHC class 1 renders mice more susceptible to EHV-1 infection.

Chapter 2

Susceptibility of rat immortalized neuronal cell line Rn33B expressing equine major histocompatibility class 1 to equine herpesvirus-1 infection is differentiation-dependent

Introduction

Equine herpesvirus-1 (EHV-1) is an alpha herpesvirus and causes encephalomyelopathy in horses. Unlike the encephalitis caused by other species of alpha herpesvirus in which the virus replicates in neurons, EHV-1 generally does not infect neurons. EHV-1 infects endothelial cells, resulting in vasculitis, thrombosis, and ischemic damage of the central nervous system (9).

Little is known about the mechanism underlying low susceptibility of neurons to EHV-1 infections due to the lack of reliable and convenient cell culture systems. Murine neuronal cell lines, which have been used in experimental infection of herpes simplex virus-1 (HSV-1), are not suitable as a model for EHV-1 infection *in vitro*, because murine cells are resistant to EHV-1 due to the lack of a functional viral entry receptor (23).

Rn33B is a neuronal cell line derived from rat medullary raphe cells by infection with a retrovirus encoding the temperature-sensitive mutant of the SV40 large T antigen (39). Rn33B cells differentiate into neuronal cells at 37 °C (differentiated cells) and remain undifferentiated at temperatures lower than 33 °C (undifferentiated cells) (39). Because differentiated cells cease dividing and exhibit neuronal markers, they are similar to mature neurons (39).

Equine major histocompatibility class 1 (equine MHC class 1) has been reported to act as a viral entry receptor and render murine cells susceptible to EHV-1 infection (23,24). In this study, an Rn33B-derived cell line that constitutively expresses equine MHC class 1 (Rn33B-A68B2M) was established to create a convenient model for studying the susceptibility of neurons to EHV-1 infection. As such, the susceptibility of undifferentiated Rn33B-A68B2M cells with EHV-1 infection was compared with that of

differentiated counterparts. As the host factors may be responsible for the observed differences, the effects of interferon (IFN) response and the components of a transcriptional regulatory complex on the viral immediate-early promoters (i.e. Oct-1 and HCF-1) were also investigated. The latter is known to be vital for the initiation of HSV-1 transcription in neurons (40).

Materials and methods

Cells and viruses

RK13 and Vero cells were cultured in Eagle's minimum essential medium (EMEM; Nissui, Tokyo, Japan) containing 10% fetal bovine serum (FBS). E.Derm and 293T cells were cultured in Dulbecco's modified EMEM (DMEM; Nissui) containing 10% FBS and MEM Non-essential Amino Acids Solution (FUJIFILM Wako Pure Chemical Corporation, Osaka, Japan). Undifferentiated Rn33B and Rn33B-A68B2M cells were maintained in DMEM / Ham's F-12 (Nissui) containing 10% FBS at 32 °C. For differentiation, Rn33B and Rn33B-A68B2Mcells were cultured at 37 °C in DMEM high glucose / Ham's F12 containing 1% bovine serum albumin (FUJIFILM Wako Pure Chemical Corporation) and N_2 supplement (FUJIFILM Wako Pure Chemical Corporation). The EHV-1 strain Ab4 and EHV-1 mutant Ab4-GFP containing a green fluorescent protein (GFP) expression cassette between ORF 62 and 63 were produced in E.Derm cells and titrated by plaque formation assay in RK13 cells (30,41). HSV-1 (F) were cultured in Vero cells for the stock.

Plasmids

The self-inactivating (SIN) lentiviral vector construct (pCSII-CMV-MCS-IRES2-Bsd), packaging construct (pCAG-HIVgp), and the VSV-G and Rev-expression construct (pCMV-VSV-G-RSV-Rev) were kindly provided by Dr Miyoshi (RIKEN Bio Resource Center, Ibaraki, Japan). The DNA fragment containing the equine MHC class 1 heavy chain *A68* gene (GenBank/EMBL/DDBJ entry AB525079) and downstream *equine β2-microglobulin* (*β2m*) gene was amplified from plasmid pCAGGS-V68-2A-

B2M by using NheI-A68F and EcoRI-A68R as primers, and the fragment was cloned into the *Nhe*I-*Eco*RI site of the pCSII-CMV-MCS-IRES2-Bsd vector (42). A recombinant lentivirus vector was generated by transient transfection of 293T cells with a combination of pCAG-HIVgp and pCMV-VSV-G-RSV-Rev. The supernatant containing the lentiviral vector was collected after the incubation of the cells at 37 °C for 48 hr. Rn33B cells were infected with the lentiviral vector and cultured in the presence of 5 μg/ml blasticidin-S (MERCK). PCR primers used in this study are listed in Table 2.

Flow cytometry

Undifferentiated and differentiated Rn33B-A68B2M cells were cultured at 32 ºC and 37 ºC, respectively. Two days after the culture, cells were collected using Cell Dissociation Buffer, Enzyme-Free, PBS-based (Thermo Fisher SCIENTIFIC). Cells were incubated with the anti-equine MHC class 1 monoclonal antibody PT85A (1/200 dilution, WSU monoclonal antibody center, Washington, USA) at 4 °C for 30 min. Mouse IgG2a (1/200 dilution, BioLegend, California, USA) was used as a control. Cells were stained with allophycocyanin (APC)-conjugated anti-mouse IgG antibody (1/200 dilution, BioLegend) at 4 °C for 30 min. Flow cytometry was performed using a BD FACSVerse^{TM} system (BD Biosciences, New Jersey, USA), and the data collected was analyzed using the FCS express 4 software(De Novo Software, California, USA).

Real-time PCR

Cells were collected, and total RNA was extracted using the TriPure isolation reagent (MERCK). cDNA was synthesized using the previously extracted RNA as a

template by using the PrimeScript^{TM} II 1st strand cDNA synthesis kit (Takara, Shiga, Japan). cDNA (0.5 μl) was used in the final reaction volume of 5 μl and the experiment was performed in triplicate using the KAPA SYBR FAST qPCR Master Mix ABI Prism^{TM} (Roche, Basel, Switzerland) in a Step One^{TM} Real-Time PCR system (Thermo Fisher SCIENTIFIC). The real-time PCR program was 1 cycle of 95 °C for 3 min and 40 cycles of 95 °C for 3 sec and 60 °C for 30 sec. As an internal control, rat *β-actin* was used. The C_T value of the target genes was normalized by that of internal controls, and then the expression levels of genes in undifferentiated cells were compared with those in differentiated cells using the $2^{-\Delta\Delta C_T}$ method (43). Primers used in this study are shown in Table 2.

Reverse transcription-polymerase chain reaction (RT-PCR)

Cells were infected with the virus at a multiplicity of infection (MOI) of 5. Cells transfected with poly(deoxyadenylic-deoxythymidylic) (poly(dA:dT); MERCK) using Lipofectamine 3000 (Thermo Fisher SCIENTIFIC) were used as positive controls for IFN response. Total RNA was extracted using the TriPure isolation reagent. After the treatment with amplification-grade DNase I (Thermo Fisher SCIENTIFIC), RNA was converted into complementary DNA with the PrimeScript^{TM} II 1st strand cDNA synthesis kit. To detect transcripts, PCR was performed with primers specific for *ICP0*, *gB*, *IFN-α*, *IFN-β*, and *β-actin* genes using a previously described method (29,44). The band density was measured using ImageJ software. The band density of viral transcripts was divided by that of internal controls. The mean densities of the bands were statistically compared using the Tukey-Kramer test for the *ICP0* gene and Student's *t*-test for the *IFN-α* gene.

Viral growth analysis

Cells were infected with EHV-1 Ab4 or HSV-1 (F) at an MOI of 5. After incubation at 37 °C for 1 hr, cells were washed with Glycine buffer (0.05 M glycine-HCl, 0.1 M NaCl, pH 3.0) and cultured with growth medium. At 1, 8, 24, and 48 hr p.i., the cells were collected and sonicated. The viral titer was determined by the plaque formation assay on RK13 cells for EHV-1 or on Vero cells for HSV-1 (F).

Immunofluorescence analysis

Cells were cultured at temperatures below 32 °C for undifferentiated cells or at 37 °C for differentiated cells in poly-L-lysine-pretreated dishes for 2 days. 293T cells were used as a reference. Two days after the culture, the cells were fixed with 4% paraformaldehyde for 15 min and then permeabilized by using 0.1% TritonX-100 for 10 min at room temperature. Cells were stained with rabbit polyclonal anti-HCF-C1 antibody (1/50 dilution, Proteintech, IL, USA) followed by Alexa 488 conjugated anti-rabbit IgG (1/1000 dilution, Thermo Fisher SCIENTIFIC). Nuclei were counterstained with Hoechst 33258 (MERCK). Fluorescence was detected using an LSM 700 confocal microscope.

Western blot

Cells were lysed with RIPA buffer (50mM Tris-HCl (pH 8.0), 150mM NaCl, 0.5% DOC, 0.1% SDS, and 1% NP-40) containing a complete protease inhibitor cocktail (Merck), and then were sonicated. The lysates were separated by SDS-PAGE and were transferred to Immobilon-P membranes. The membranes were blocked for 1hr

in 5% BSA in TBST, and then incubated with a primary antibody at 4 ºC overnight. The primary antibody was detected with an HRP-conjugated second antibody. Signals were visualized by using Immobilon Western Chemiluminescent HRP Substrate (Merck Millipore). Beta-actin was used as an internal control. The antibodies used in this study were as follows: Phospho-Stat1 (Tyr701) (D4A7) Rabbit mAb (1/1000 dilution, Cell Signaling Technology, Massachusetts, USA), Stat1 antibody (1/1000 dilution, Cell Signaling Technology), rabbit polyclonal anti-OCT-1 antibody (1/1000 dilution, Proteintech), rabbit polyclonal anti-HCF-C1 antibody (1/500 dilution, Proteintech), Anti-Actin Antibody, clone C4 (1/10000 dilution), anti-Mouse IgG, HRP-Linked Whole Ab Sheep (1/10000 dilution, GE Healthcare UK Ltd., Little Chalfont, England), and Anti-Rabbit IgG, HRP-Linked Whole Ab Donkey (1/10000 dilution, GE Healthcare UK Ltd.).

Results

Establishment of a rat neuronal cell line expressing equine MHC class 1

To establish a susceptible cell line to EHV-1 infection, Rn33B cells were lentivirally transduced with the clone 68 of the equine MHC class 1 heavy chain gene and horse b2-microglobulin (Rn33B-A68B2M cells) (23,24). As Rn33B cells proliferate at a permissive temperature of 32 ºC, proliferation is stopped and differentiation is induced when cells are cultured under a non-permissive temperature of 37 ºC (39). Differentiated Rn33B-A68B2M as well as Rn33B cells, exhibited a bipolar shape with round cell bodies and unbranched fibers (Fig. 6a). In the present study, when compared to undifferentiated cells cultured under permissive temperatures, differentiated cells expressed low affinity of the nerve growth factor (NGF) receptor, which is a neuronal marker (Fig. 6b). The expression of equine MHC class 1 was detected in undifferentiated and differentiated Rn33B-A68B2M cells but was not detected in either type of Rn33B cells (Fig. 6c).

Susceptibility of Rn33B-A68B2M cells to EHV-1 infection

To confirm the susceptibility of Rn33B-A68B2M cells to EHV-1 infection, cells were infected with Ab4-GFP virus at 37 ºC and then incubated under 32 ºC for undifferentiated cells or 37 ºC for differentiated cells (Fig. 7a). E.Derm, a cell line susceptible to EHV-1 infection, was used as a positive control. Undifferentiated Rn33B-A68B2M and E.Derm cells displayed GFP expression at 8, 12, and 48 hr p.i., while undifferentiated Rn33B cells showed no GFP expression (Figs. 7b, c, d, and f). This indicates that equine MHC class 1 renders Rn33B cells susceptible to EHV-1 infection.

Interestingly, GFP signals were not detected in differentiated Rn33B-A68B2M cells (Figs. 7e and f). At 48 hr p.i., syncytial cells were observed in undifferentiated Rn33B-A68B2M cells. However, their differentiated counterparts showed no syncytial formation (Fig. 7g). To characterize viral gene expression in Rn33B-A68B2M cells, RT-PCR for the *ICP0* (early gene) and *gB* (late gene) genes of EHV-1 was performed. At 1 hr p.i., no viral RNA was detected in undifferentiated and differentiated cells (Fig. 7h). Starting from 4 hr p.i., the expression of ICP0 and gB was detected in undifferentiated cells, while the expression of the ICP0 and gB genes in differentiated cells was lower and undetectable, respectively (Fig. 7h). The expression of the viral RNAs examined was detected in E.Derm cells, while they were not observed in Rn33B cells (Fig. 7h).

To examine the ability of undifferentiated and differentiated cells to support EHV-1 replication, undifferentiated and differentiated cells were infected with EHV-1 Ab4 at 37 ºC, and then incubated under permissive or non-permissive condition, respectively (Fig. 7a). RK13 cells, which are known to be highly susceptible to EHV-1 infection were used as a reference. The titer of EHV-1 in undifferentiated cells gradually increased with time, while differentiated cells yielded no infectious progeny (Fig. 8a). To evaluate whether differences in expression level of equine MHC class 1 between undifferentiated and differentiated cells affected on EHV-1 production, undifferentiated cells were infected with EHV-1 Ab4, and then cultured at 32 ºC (to maintain undifferentiated) or 37 ºC (to induce differentiation). Plaque forming assay revealed that EHV-1 production was observed in the former, not in the latter (data not shown). These results indicate that differentiated cells are far less susceptible to EHV-1 infection than their undifferentiated counterparts.

To confirm whether temperature affected the differences in the amount of viral

replication, RK13 cells infected with EHV-1 Ab4 were cultured at 32 or 37 ºC. There was no difference in the peak level of viral replication at 32 or 37 ºC in RK13 cells (Fig 8b). This result indicates that decreased susceptibility of differentiated cells to EHV-1 occurs independently of temperature.

Susceptibility of Rn33B cells to HSV-1

HSV-1, which is a member of the alpha herpesvirus family, causes encephalitis in humans. Mouse are susceptible to HSV-1 and have been used as experimental models for HSV-1 infections (20,45,46). Thus, the effect of differentiation of RN33B cells on their susceptibility to HSV-1 infection. The plaque forming assay using HSV-1 revealed that, although the peak level of viral titer in undifferentiated was higher than those of differentiated cells, differentiated cells, as well as undifferentiated cells, supported the production of infectious viral progeny (Fig. 8c). These results suggest that both undifferentiated and differentiated Rn33B cells are susceptible to HSV-1 infection.

Expression of Oct-1 and HCF-1 in Rn33B-A68B2M cells

The assembly of a transcriptional regulatory complex on the viral immediate-early promoters is required for the initiation of viral transcription in herpesviruses (40). The transcriptional regulatory complex includes two host cellular proteins, Oct-1 and HCF-1. Reduced expression of Oct-1 and/or cytoplasmic localization of HCF-1 impedes the formation of the transcriptional regulatory complex in the nucleus, followed by inhibition of viral lytic gene expression (47).

Because EHV-1 transcription was restricted in differentiated cells, the expression of Oct-1 and HCF-1 was examined using real-time PCR, western blot and

immunofluorescent staining. Expression of Oct-1 and HCF-1 was detected in differentiated cells as well as in their undifferentiated counterparts (Fig. 9a). Differentiated and undifferentiated cells expressed Oct-1 and HCF-1 proteins (Fig. 9b). Immunofluorescent staining revealed the localization of HCF-1 in the nucleus and cytoplasm of undifferentiated and differentiated cells (Figs. 9c and d). These results suggest that the restriction of EHV-1 gene transcription in differentiated cells is not due to the paucity of the cellular component of the transcriptional regulatory complex.

Interferon response to EHV-1 in Rn33B-A68B2M cells

Because the secretion of type 1 IFN is a characteristic response to viral infection, the IFN response was investigated to confirm whether immune response made the differences in the susceptibility to EHV-1 infection between undifferentiated and differentiated cells. The expression of IFN-α and IFN-β in the cells infected with Ab4 was determined by RT-PCR. Cells transfected with poly (dA:dT) were used as references. At 12 hr p.i., EHV-1 infection in differentiated cells induced higher levels of IFN-α transcription, compared with that of undifferentiated cells (Fig. 10a). Transcription of IFN-β was not detected in either undifferentiated or differentiated cells infected with EHV-1 (Fig. 10a). After IFNs bind to the IFN-α/β receptors, production of a variety of interferon stimulated genes (ISGs) is induced through the activation of the JAK-STAT pathway. STAT1 is a key component of the JAK-STAT signaling pathway and is activated through phosphorylation. As such, the phosphorylation of STAT1 and the expression of ISGs were investigated by western blot and real-time PCR, respectively. Neither phosphorylated STAT1 nor ISGs, including ISG15 and ISG54, were detected in undifferentiated and differentiated cells (Figs. 10b and c). These results

suggest that the IFN response is unlikely to contribute to the reduction in the susceptibility to EHV-1 infection of differentiated cells.

Discussion

In the present study, a rat neuronal cell line RN33B-A68B2M expressing an EHV-1 entry receptor was established. Differentiated cells showed a bipolar shape and increased expression of neuronal markers. Undifferentiated cells supported EHV-1 replication, while differentiated cells did not produce progeny virus. These results suggest that neuronal differentiation of Rn33B-A68B2M cells reduces susceptibility to EHV-1 infection.

HSV-1 replication in differentiated cells observed in the present study is consistent with the neurotropic nature of HSV-1. Mice infected with HSV-1 showed encephalitis, which results from neuronal damage induced by the virus (46). PC-12, a rat neuronal cell line, has been reported to be susceptible to HSV-1 and is used as a model of neuronal infection *in vitro* (20,21). Unlike HSV-1, differentiated cells did not support EHV-1 replication, suggesting that strong inhibition of viral replication in differentiated Rn33B-A68B2M cells may be a specific event that occurs in EHV-1 infection.

The responsible factors which contribute to the reduced susceptibility of differentiated cells are still unknown. The IFN response suppresses viral replication. Notably, while the IFN-α expression levels were increased in differentiated cells infected with EHV-1, neither phosphorylation of STAT1 nor expression of ISGs were observed. The assembly of a transcriptional regulatory complex on the viral immediate-early promoters is vital for the initiation of viral transcription in HSV-1 (40). The transcriptional regulatory complex is composed of one viral protein, VP16, and two host cellular proteins, Oct-1 and HCF-1 (40). In neurons, a decrease in Oct-1 expression and

localization of HCF-1 in the cytoplasm results in the inhibition of HSV-1 transcription (40,47). In this study, EHV-1 transcription was found to be repressed in differentiated cells. However, Oct-1 expression levels in differentiated and undifferentiated cells were shown to be identical. Moreover, HCF-1 was localized in the nucleus regardless of whether cells were differentiated or not. These results suggest that the IFN response and the transcriptional regulatory complex are not the factors underlying the differentiation-dependent susceptibility of Rn33B-A68B2M to EHV-1 infection. Because the expression of EGFP was not observed after the infection of differentiated Rn33B-A68B2M cells with Ab4-GFP, viral entry processes such as fusion of the viral envelope with plasma membrane or endosomal membrane, transport of capsid along microtubules, docking of capsid at nuclear pore complex and subsequent DNA transport into the nucleus may be impaired (Fig. 11) (48,49). Decreased expression of equine MHC class 1 on the cell surface of differentiated cells may be responsible, at least in part to decreased viral entry in the differentiated cells.

The susceptibility of murine neurons to EHV-1 infection is still controversial. EHV-1 infects neurons in suckling mice and causes neuronal damage (50,51). However, neurons in adult mice are spared after experimental infection with EHV-1 (52–54). While George *et al.* (54) suggest that cell-mediated immune responses prevent viral widespread in the brain of adult mice, neuronal maturation is likely to be involved in the decrease in EHV-1 replication in adult mouse brains. The reduced susceptibility of differentiated Rn33B-A68B2M cells observed in this study, which mimics the properties of EHV-1 infection in murine immature and mature neurons *in vivo*, suggests a maturation state-specific resistance of neurons to EHV-1.

In conclusion, the present study examined the susceptibility of undifferentiated

and differentiated Rn33B-A68B2M cells to EHV-1, and found that the cells become resistant to infection as they underwent neuronal differentiation. Due to the fact that Rn33B-A68B2M can be induced to differentiate by a simple method (i.e. culture at non-permissive temperature), it provides a convenient model for studying the molecular mechanism underlying neuron-specific resistance to EHV-1 infection *in vitro*.

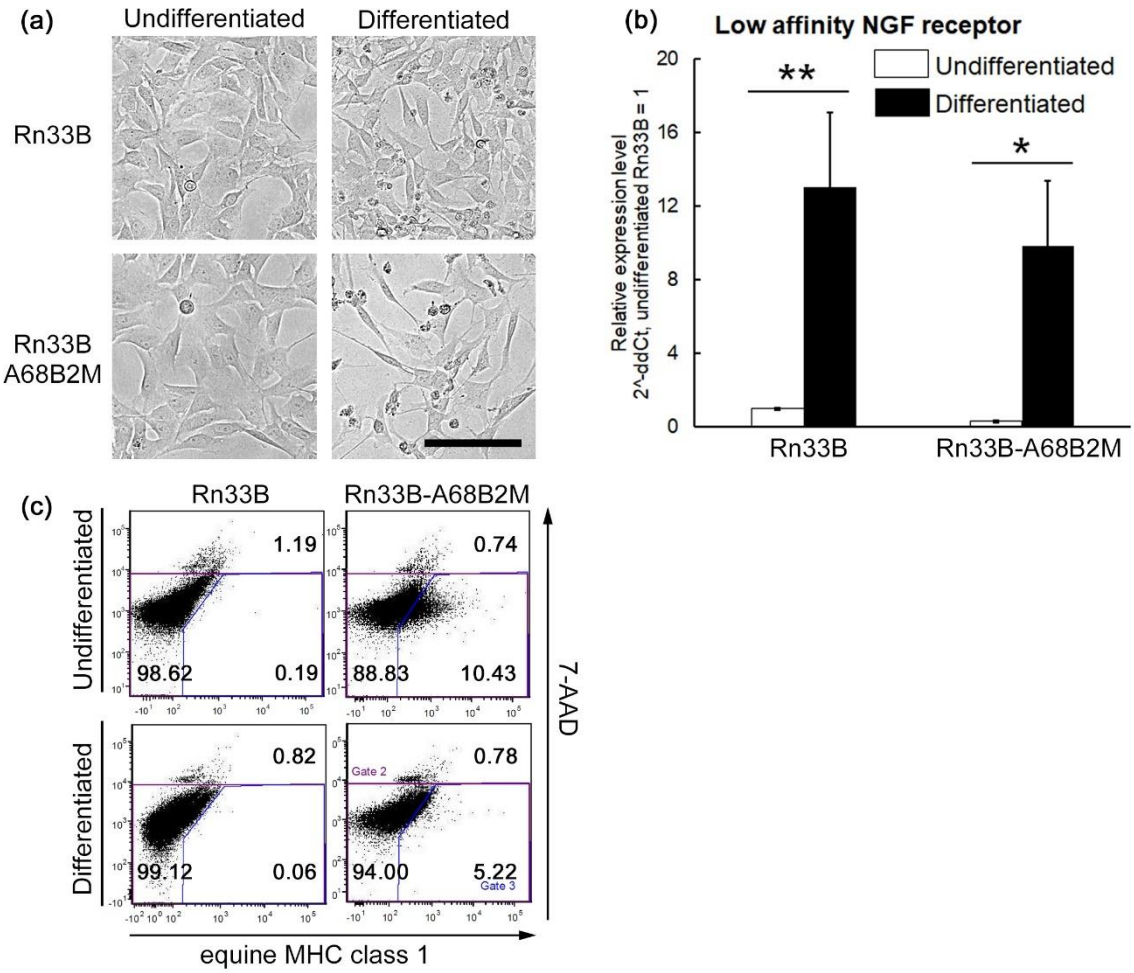

Figure 6. Establishment of rat neuronal cell line expressing equine MHC class 1.

Cells were cultured at 32 °C for undifferentiated cells or 37 °C for differentiated cells. Rn33B-A68B2M: Rn33B cells transduced with equine MHC class 1. (a) Morphology of undifferentiated and differentiated cells. Bar = 100 µm. (b) Expression of low affinity NGF receptor in undifferentiated and differentiated cells. Transcripts of the low affinity NGF receptor were quantified using real-time PCR. Bars represent means and standard deviations from three independent experiments. Rn33B cells were used as a reference. * $p < 0.05$, ** $p < 0.01$, Tukey-Kramer test. (c) Flow cytometry detection of equine MHC class 1 on undifferentiated and differentiated cells. Cells were stained with anti-equine MHC class 1 antibody. 7-AAD was used to exclude dead cells.

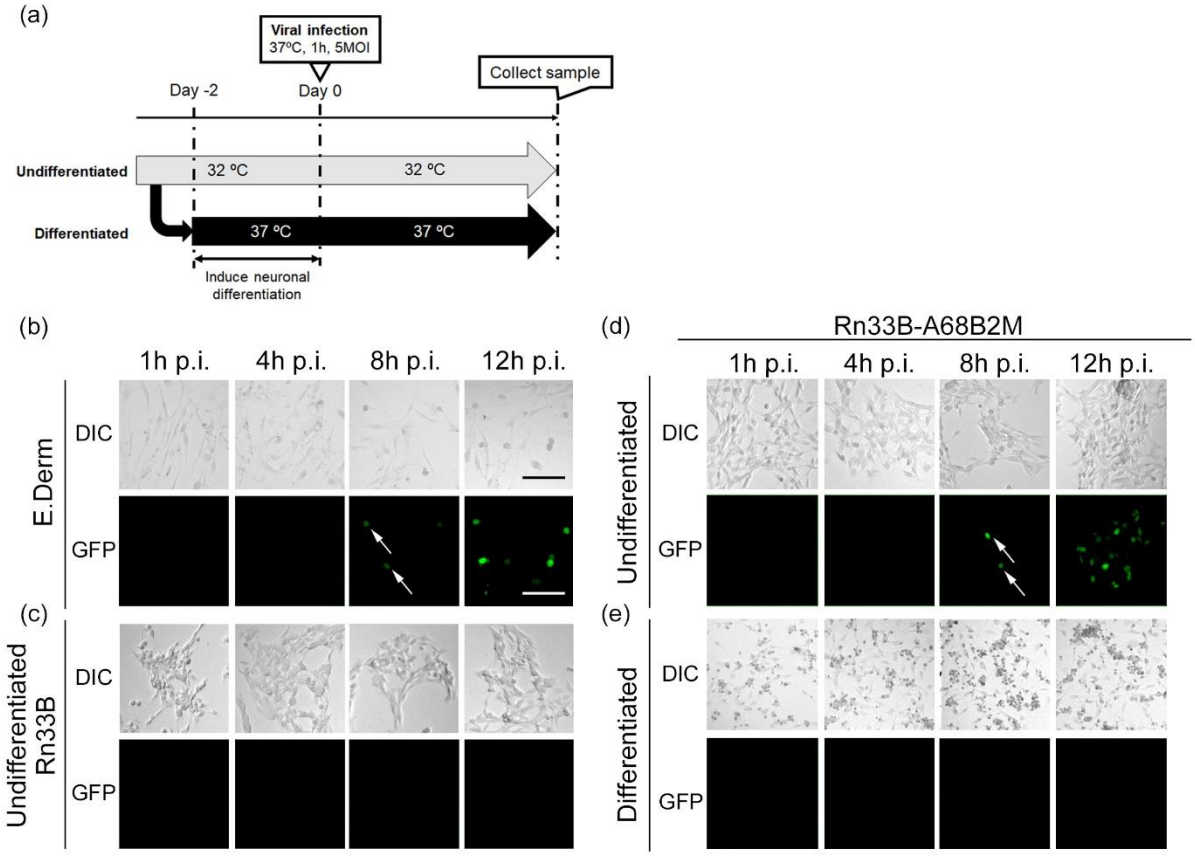

Figure 7. Differentiation-dependent susceptibility of Rn33B-A68B2M cells to EHV-1 infection.

Cells were infected with Ab4-GFP at an MOI of 5 for 1 hr. E.Derm was used as a reference. (a) Scheme of the experiment. (b-e) Microscopic detection of cells expressing GFP at 1, 4, 8, and 12 hr p.i. in (b) E.Derm cells, (c) undifferentiated Rn33B cells, (d) undifferentiated Rn33B-A68B2M cells, and (e) differentiated Rn33B-A68B2M cells. Arrows indicate cells expressing GFP. DIC: differential interference contrast. Bars = 250 μm.

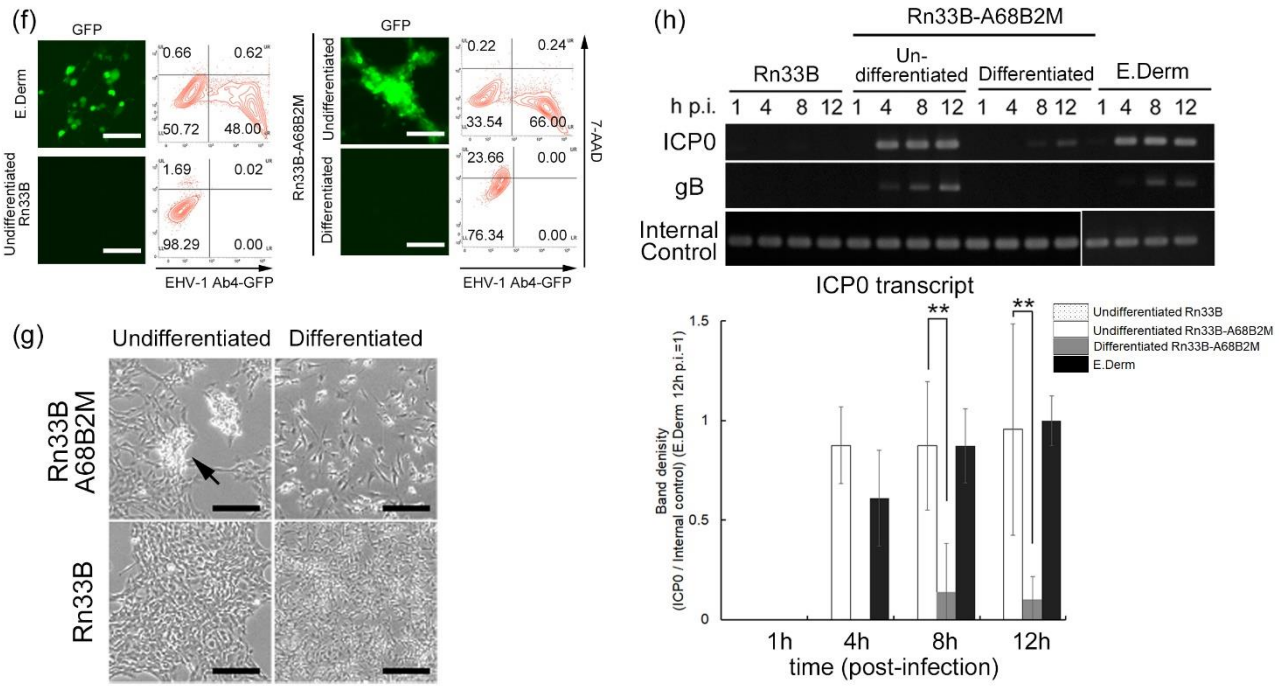

Figure 7. (f) Microscopic detection of GFP-positive cells at 48 hr p.i.. Bars = 125 μm. The number of GFP-positive cells was simultaneously quantified by flow cytometry. 7-AAD was used to exclude dead cells. (g) Morphological changes of cells infected with Ab4-GFP virus. Arrow indicates syncytial cells. Bars = 250 μm. (h) Expression of viral transcripts in Rn33B-A68B2M cells. *ICP0*: viral early gene, *gB*: viral late gene. *β-actin* was used as an internal control. Band density of the ICP0 transcript was calculated using the Image J software. Bars represent means and standard deviations from three independent experiments. Statistical analysis was performed at each time point using the Tukey-Kramer test, ** $p < 0.01$.

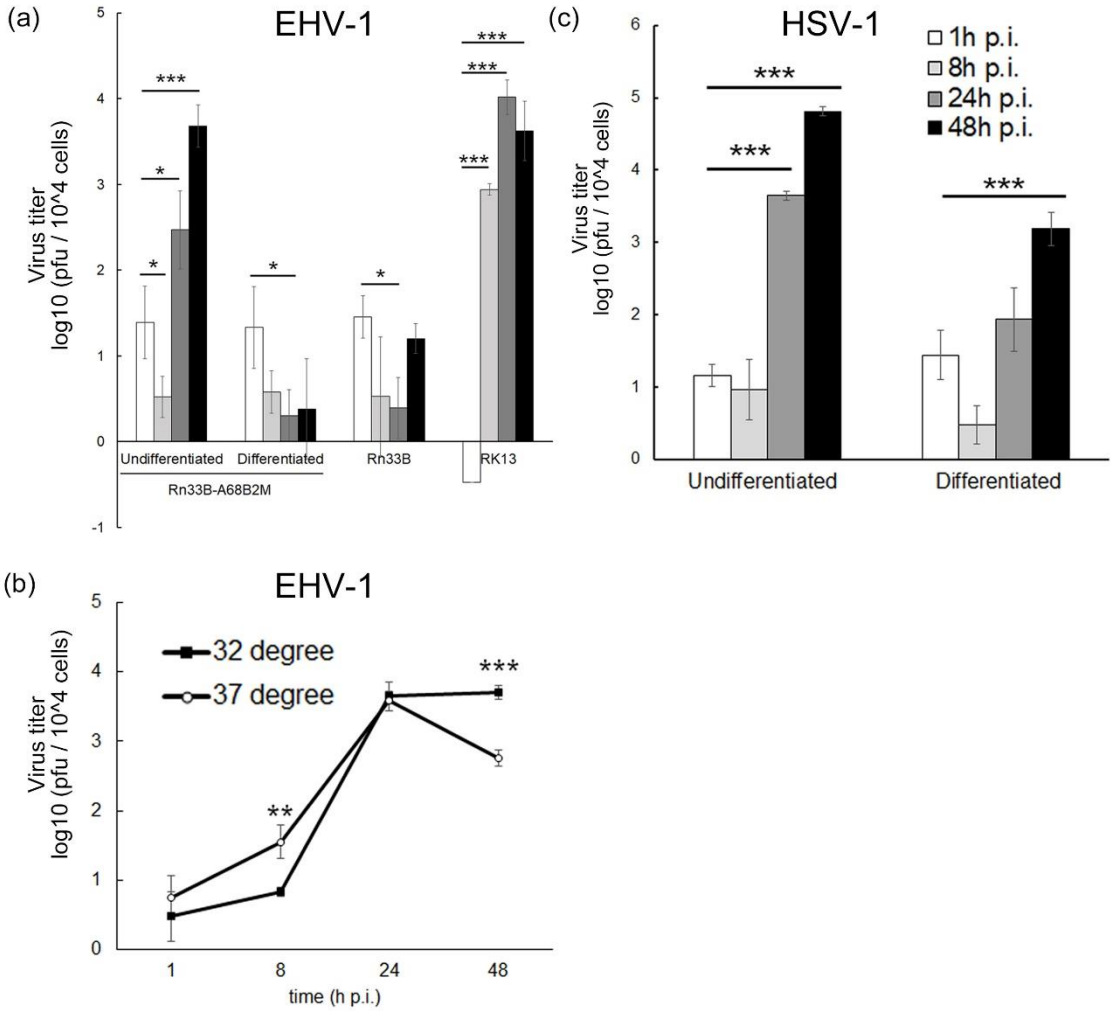

Figure 8. Growth kinetics of EHV-1 and HSV-1.

Cells were infected with (a, b) EHV-1 Ab4 or (c) HSV-1 (F) for 1 hr at an MOI of 5, and cells were collected at 1, 8, 24, and 48 hr p.i.. Bars represent means and standard deviations from three independent experiments. (a, c) Dunnett's test, (b) Student's *t*-test, * $p < 0.05$, ** $p < 0.01$, *** $p < 0.001$.

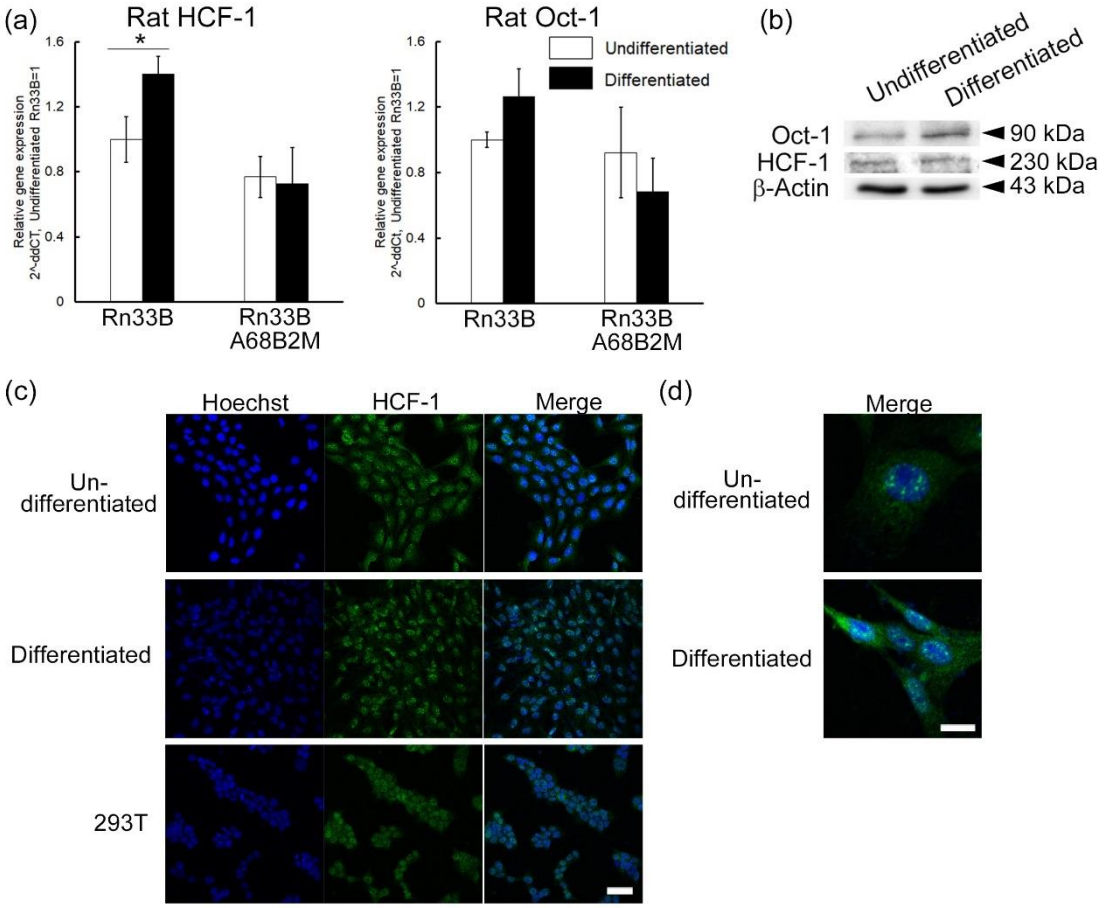

Figure 9. Expression of HCF-1 and Oct-1 in Rn33B-A68B2M cells.

(a) Transcription of *HCF-1* and *Oct-1* was quantified by real-time PCR. Bars represent means and standard deviations from three independent experiments. * $p < 0.05$, Student's *t*-test. (b) Expression of Oct-1 and HCF-1 protein in Rn33B-A68B2M cells. b-actin was used as an internal control. (c, d) Localization of HCF-1 in Rn33B-A68B2M cells was confirmed by immunofluorescent staining. 293T was used as a reference. Cells were stained with rabbit polyclonal anti-HCF-C1 antibody, followed by Alexa 488-conjugated anti-rabbit IgG. The nucleus was stained with Hoechst 33258. (c) Bar = 50 μm. (d) Bar = 20 μm.

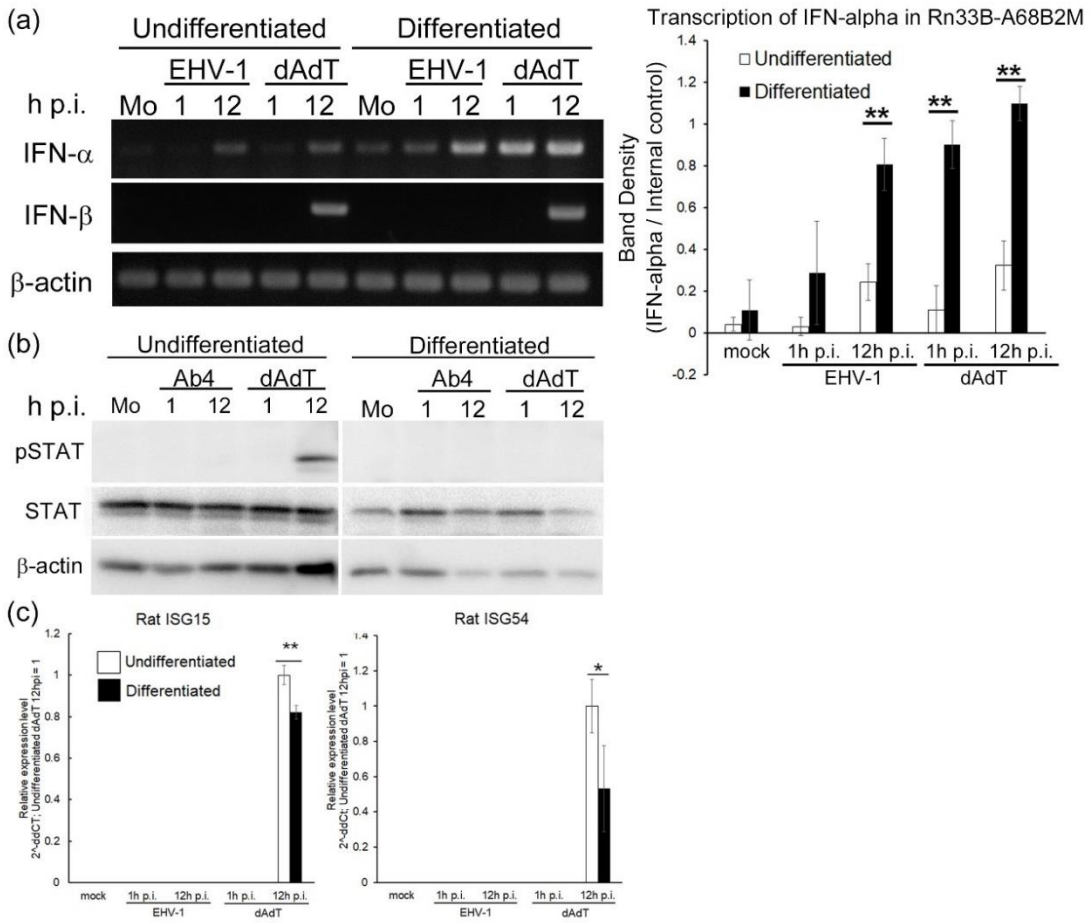

Figure 10. Reduced IFN response to EHV-1 infection in Rn33B-A68B2M cells.

Rn33B-A68B2M cells were infected with EHV-1 Ab4 for 1 hr at an MOI of 5. Cells transfected with poly (dA:dT) were used as a reference. Mo: mock infected cells, EHV-1: cells infected with EHV-1 Ab4, dA:dT: cells transfected with poly (dA:dT). (a) Transcription of type 1 IFN was detected by RT-PCR. Rat *β-actin* was used as an internal control. Band density of *IFN-α* was calculated using the Image J software. Bars represent means and standard deviations from three independent experiments. ** $p < 0.01$, Student's *t*-test. (b) Detection of phosphorylated STAT1 by western blot. Beta-actin was used as an internal control. (c) Transcription of ISGs was quantified using real-time PCR. Bars represent means and standard deviations from three independent experiments. * $p < 0.05$, ** $p < 0.01$, Student's *t*-test.

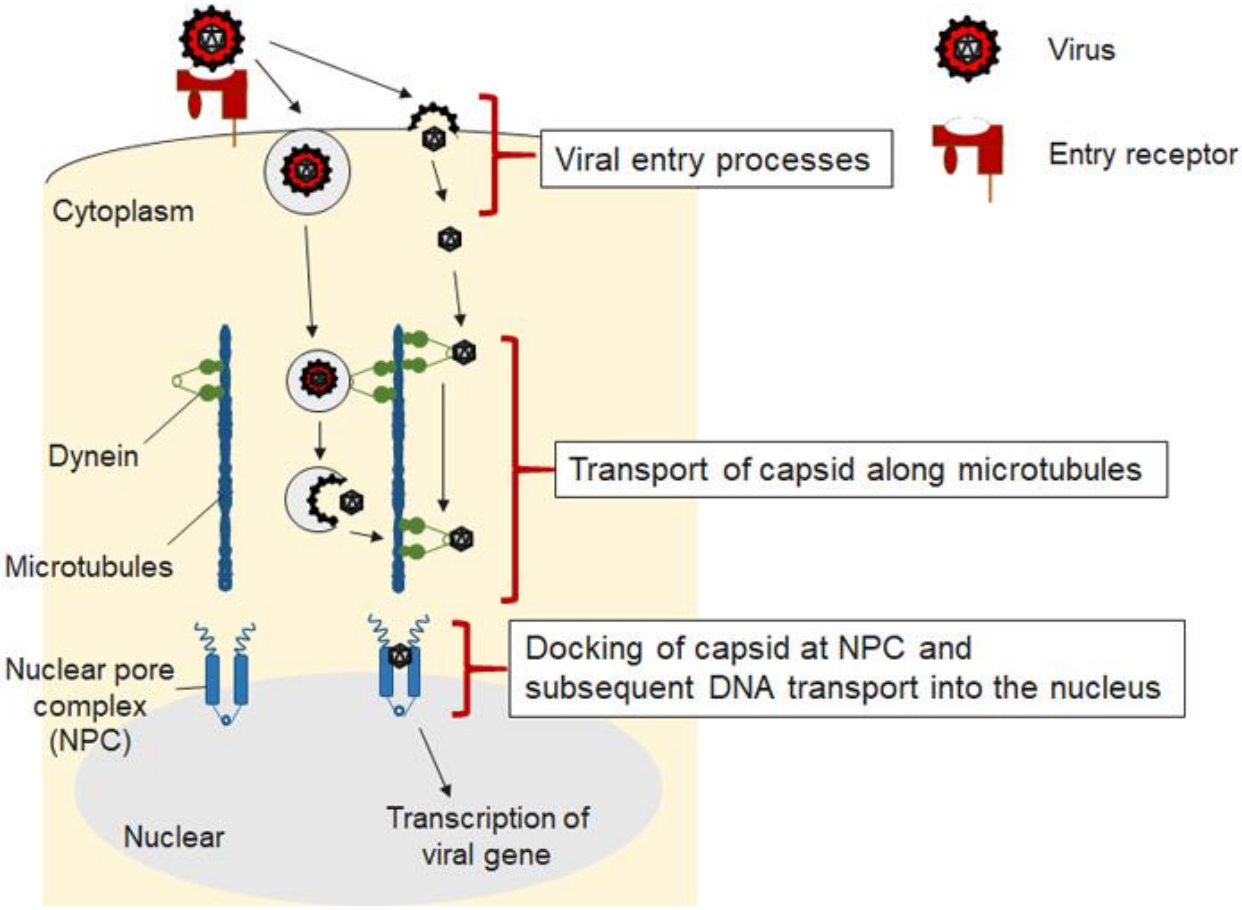

Figure 11. Viral interaction with the microtubules and nuclear pore complex (NPC).

Following viral entry through endocytosis or direct fusion, virus interacts with microtubules and dynein to transport of capsid along microtubules. Docking of capsid at NPC results in viral DNA transport into the nucleus (modification of Wang IH *et al*. Viruses, 2018) (48).

Table 2. Primer sequences

primer name	alignment (5' to 3')	
NheI-A68F	ACGTGCTAGCACCATGTGGGTCATGGAG	(28 bp)
EcoRI-A68R	ATGTGAATTCTCAGAGGTCTCGATCCCAC	(29 bp)
Rat_p75NTR_F	GCTGATGCTGAATGCGAAGAG	(21 bp)
Rat_p75NTR_R	TGGGTACAAGGTCTTGCTCTG	(21 bp)
Rat_actin_qpcr_F	AGGCCAACCGTGAAAAGATG	(20 bp)
Rat_actin_qpcr_R	TGGATGGCTACGTACATGGC	(20 bp)
Rat HCF-1_F	TGGAAAAGCTCCTGTCACTGTG	(22 bp)
Rat HCF-1_R	ATCTGTGGGTTGCTGCCAATC	(21 bp)
Rat Oct-1_F	TTCAGTGCAGTCAGCCATTCC	(21 bp)
Rat Oct-1_R	TGGGCCTGCTGTAGTAAAAGC	(21 bp)

bp: base pair

Summary

Equine herpesvirus-1 (EHV-1), which causes encephalomyelitis in horses, shows endotheliotropism in the central nervous system of horses, and generally does not infect neurons. However, little is known about the mechanism underlying the resistance of neurons to EHV-1, due to the lack of convenient cell culture systems. In this study, EHV-1 infection in immortalized Rn33B rat neuronal cells was examined. Rn33B cells are known to differentiate into neurons when cultured under non-permissive conditions. Because murine cell lines showed resistances to EHV-1 due to the lack of functional entry receptors for EHV-1, Rn33B cells were transduced with equine major histocompatibility class 1 molecule, which acted as EHV-1 entry receptor (Rn33B-A68B2M cells). EHV-1 infected undifferentiated Rn33B-A68B2M cells more efficiently than differentiated cells, resulting in the production of progeny virus in the former but not in the latter. In contrast, both differentiated and undifferentiated cells supported herpes simplex virus-1 production. While EHV-1 infection induced stronger expression of interferon (IFN) alpha gene in differentiated cells than in undifferentiated cells, downstream IFN responses (i.e. phosphorylation of STAT1, expression of IFN-stimulated genes) were not activated regardless of whether cells were differentiated or not. These results suggest that neuronal differentiation of RN33B-A68B2M cells reduced their susceptibility to EHV-1, which is not due to the differences in IFN responses. This culture system may be useful as a model for studying neuron-specific resistance to EHV-1 *in vitro*, by investigating viral and host factors responsible for the difference in susceptibility between differentiated and undifferentiated cells.

Conclusion

EHV-1, an alphaherpesvirus, causes respiratory diseases, abortions and neurological symptoms in horses, resulting in severe economic losses in horse industries. While vaccines are used to protect horses from EHV-1 infection, outbreaks of EHV-1 have been reported around the world.

Because experimental infection using horses is expensive and labour-intensive, small animal models and *in vitro* infection models are needed to be developed. Mice are often used in experimental infection with EHV-1, but mouse models do not reproduce important aspects of EHV-1 infection such as the development of myeloencephalopathy. Limited number of EHV-1-susceptible cell culture models also disturbs us to study cell type-specific host response to EHV-1 infection. Especially, mechanisms underlying the resistance of neurons to EHV-1 infection has not been investigated, due to the lack of neuronal cell culture model.

To overcome the paucity of infection models available, a mouse model and a rat neuronal cell line were generated by transduction with a functional entry receptor for EHV-1 which conferred the EHV-1-susceptibility. In chapter 1, mice ubiquitously expressing equine MHC class 1 was generated and the susceptibility of transgenic mice to EHV-1 was confirmed. Various organs including the lung of Tg mice expressed equine MHC class 1. Experimental nasal infection with EHV-1 demonstrated that more cells were infected with EHV-1 in the lung of Tg than that of WT mice. These findings demonstrate that transgenic expression of equine MHC class 1 increases the susceptibility of mouse cells to EHV-1 *in vivo*.

In chapter 2, a rat neuronal cell line RN33B-A68B2M expressing an equine

MHC class 1 was established to confirm whether neurons were susceptible to EHV-1 or not. Rn33B-A68B2M cells remained undifferentiated at 32 ºC and neuronally differentiated at 37 ºC, which was identical to parental cell line Rn33B. While undifferentiated Rn33B-A68B2M cells supported EHV-1 replication, differentiated cells did not produce progeny virus. Interestingly, differentiated Rn33B cells as well as undifferentiated cells supported HSV-1 production. These results suggest that cells become resistant to EHV-1 infection as they underwent neuronal differentiation.

In this study, it was found that the expression of equine MHC class 1 effected on the development of pulmonary lesions in Tg mice infected with EHV-1 *in vivo*. The rat neuronal cell model was also developed, and the model showed differentiation-dependent susceptibility to EHV-1 infection i*n vitro*. These models may be useful to unveiling the molecular pathogenicity in EHV-1 infection.

Acknowledgements

The author would like to extend my sincerest thanks and appreciation to my supervisors Professor Takashi Kimura, Associate Professor Atsushi Kobayashi, and Assistant professor Keisuke Aoshima (Laboratory of Comparative Pathology, Faculty of Veterinary Medicine, Hokkaido University) for their mentorship and support.

The author sincerely appreciate Professor Kazuhiko OHASHI (Laboratory of Infectious Diseases, Department of Disease Control, Faculty of Veterinary Medicine, Hokkaido University), Professor Ken-ichi Otsuguro (Laboratory of Pharmacology, Department of Basic Veterinary Sciences, Faculty of Veterinary Medicine, Hokkaido University), and Assistant Professor Rie Hasebe (Institute for Genetic Medicine, Hokkaido University) for their critical review of the manuscript.

The author would like to thank Dr. Naomi Ohnishi (Project for Personalized Cancer medicine, Cancer Precision Medicine Center, Japanese Foundation for Cancer Research, Tokyo, Japan) for kindly providing the plasmid pCAGGS-MCS(KS) [chapter 1]. The author appreciate to Professor Nobuya Sasaki (Laboratory of Laboratory Animal Science and Medicine, School of Veterinary Medicine, Kitasato University, Towada, Japan) for advice on transgenic mice [chapter 1]. The author also appreciate to Professor Hideto Fukushi (Laboratory of Veterinary Microbiology, Faculty of Applied Biological Sciences, Gifu University) for kindly providing EHV-1 Ab4 and EHV-1 Ab4-GFP virus [chapter 1 and 2].

Finally, the author wish to thank all the members of the laboratory of Comparative Pathology of Veterinary Medicine, Hokkaido University, for their support.

This work was supported by Grant-in-Aid for Scientific Research (B) (Grant

no. 16H05022) from the Ministry of Education, Culture, Sports, Science, and Technology, Japan.

References

1. Vissani MA, Becerra ML, Olguín Perglione C, Tordoya MS, Miño S, Barrandeguy M. 2009. Neuropathogenic and non-neuropathogenic genotypes of Equid Herpesvirus type 1 in Argentina. Vet Microbiol 139:361–4.
2. Fritsche AK, Borchers K. 2011. Detection of neuropathogenic strains of Equid Herpesvirus 1 (EHV-1) associated with abortions in Germany. Vet Microbiol 147:176–80.
3. Pronost S, Legrand L, Pitel PH, Wegge B, Lissens J, Freymuth F, Richard E, Fortier G. 2012. Outbreak of Equine Herpesvirus Myeloencephalopathy in France: A Clinical and Molecular Investigation. Transbound Emerg Dis 59:256–63.
4. Damiani AM, de Vries M, Reimers G, Winkler S, Osterrieder N. 2014. A severe equine herpesvirus type 1 (EHV-1) abortion outbreak caused by a neuropathogenic strain at a breeding farm in northern Germany. Vet Microbiol 172:555–62.
5. Negussie H, Gizaw D, Tessema TS, Nauwynck HJ. 2017. Equine Herpesvirus-1 Myeloencephalopathy, an Emerging Threat of Working Equids in Ethiopia. Transbound Emerg Dis 64:389–97.
6. Bryant NA, Wilkie GS, Russell CA, Compston L, Grafham D, Clissold L, McLay K, Medcalf L, Newton R, Davison AJ, Elton DM. 2018. Genetic diversity of equine herpesvirus 1 isolated from neurological, abortigenic and respiratory disease outbreaks. Transbound Emerg Dis 65:817–32.
7. Lunn DP, Davis-Poynter N, Flaminio MJ, Horohov DW, Osterrieder K, Pusterla

N, Townsend HG. 2009. Equine herpesvirus-1 consensus statement. J Vet Intern Med 23:450–61.

8. Kydd JH, Slater J, Osterrieder N, Antczak DF, Lunn DP. 2010. Report of the second havemeyer EHV-1 workshop, steamboat springs, Colorado, USA, september 2008. Equine Vet J 42:572–5.

9. Ma G, Azab W, Osterrieder N. 2013. Equine herpesviruses type 1 (EHV-1) and 4 (EHV-4)-Masters of co-evolution and a constant threat to equids and beyond. Vet Microbiol 167:123–34.

10. Kydd JH, Smith KC, Hannant D, Livesay GJ, Mumford JA. 1994. Distribution of equid herpesvirus-1 (EHV-1) in respiratory tract associated lymphoid tissue: implications for cellular immunity. Equine Vet J 26:470–3.

11. Smith KC, Whitwell KE, Mumford JA, Gower SM, Hannant D, Tearle JP. 1993. An immunohistological study of the uterus of mares following experimental infection by equid herpesvirus 1. Equine Vet J 25:36–40.

12. Edington N, Bridges CG, Patel JR. 1986. Endothelial cell infection and thrombosis in paralysis caused by equid herpesvirus-1: equine stroke. Arch Virol 90:111–24.

13. Welch HM, Bridges CG, Lyon AM, Griffiths L, Edington N. 1992. Latent equid herpesviruses 1 and 4: detection and distinction using the polymerase chain reaction and co-cultivation from lymphoid tissues. J Gen Virol 73:261–8.

14. Slater JD, Borchers K, Thackray AM, Field HJ. 1994. The trigeminal ganglion is a location for equine herpesvirus 1 latency and reactivation in the horse. J Gen Virol 75:2007–16.

15. Wilsterman S, Soboll-Hussey G, Lunn DP, Ashton LV, Callan RJ, Hussey SB,

Rao S, Goehring LS. 2011. Equine herpesvirus-1 infected peripheral blood mononuclear cell subpopulations during viremia. Vet Microbiol 149:40–7.

16. Laval K, Favoreel HW, Poelaert KC, Van Cleemput J, Nauwynck HJ. 2015. Equine Herpesvirus Type 1 Enhances Viral Replication in CD172a+ Monocytic Cells upon Adhesion to Endothelial Cells. J Virol 89:10912–23.

17. Laval K, Favoreel HW, Nauwynck HJ. 2015. Equine herpesvirus type 1 replication is delayed in CD172a + monocytic cells and controlled by histone deacetylases. J Gen Virol :118–30.

18. Bannai H, Nemoto M, Tsujimura K, Yamanaka T, Kokado H, Kondo T, Matsumura T. 2018. Comparison of protective efficacies between intranasal and intramuscular vaccination of horses with a modified live equine herpesvirus type-1 vaccine. Vet Microbiol 222:18–24.

19. Wimer CL, Schnabel CL, Perkins G, Babasyan S, Freer H, Stout AE, Rollins A, Osterrieder N, Goodman LB, Glaser A, Wagner B. 2018. The deletion of the ORF1 and ORF71 genes reduces virulence of the neuropathogenic EHV-1 strain Ab4 without compromising host immunity in horses. Ho PL, editor. PLoS One 13:e0206679.

20. Danaher RJ, Jacob RJ, Miller CS. 1999. Establishment of a quiescent herpes simplex virus type 1 infection in neurally-differentiated Establishment of a quiescent herpes simplex virus type 1 infection in neurally-differentiated PC12 cells. J Neurovirol 5:258–67.

21. Danaher RJ, Jacob RJ, Steiner MR, Allen WR, Hill JM, Miller CS. 2005. Histone Deacetylase Inhibitors Induce Reactivation of Herpes Simplex Virus Type 1 in a Latency-Associated Transcript (LAT)- Independent Manner in Neuronal Cells. J

Neurovirol 11:306–17.

22. Jiang X, Chentoufi AA, Hsiang C, Carpenter D, Osorio N, BenMohamed L, Fraser NW, Jones C, Wechsler SL. 2011. The Herpes Simplex Virus Type 1 Latency-Associated Transcript Can Protect Neuron-Derived C1300 and Neuro2A Cells from Granzyme. J Virol 85:2325–32.
23. Sasaki M, Hasebe R, Makino Y, Suzuki T, Fukushi H, Okamoto M, Matsuda K, Taniyama H, Sawa H, Kimura T. 2011. Equine major histocompatibility complex class I molecules act as entry receptors that bind to equine herpesvirus-1 glycoprotein D. Genes to Cells 16:343–57.
24. Sasaki M, Kim E, Igarashi M, Ito K, Hasebe R, Fukushi H, Sawa H, Kimura T. 2011. Single Amino Acid Residue in the A2 Domain of Major Histocompatibility Complex Class I Is Involved in the Efficiency of Equine Herpesvirus-1 Entry. J Biol Chem 286:39370–8.
25. Seliger B, Harders C, Lohmann S, Momburg F, Urlinger S, Tampé R, Huber C. 1998. Down-regulation of the MHC class I antigen-processing machinery after oncogenic transformation of murine fibroblasts. Eur J Immunol 28:122–33.
26. Herrmann F, Lehr HA, Drexler I, Sutter G, Hengstler J, Wollscheid U, Seliger B. 2004. HER-2/neu-mediated regulation of components of the MHC class I antigen-processing pathway. Cancer Res 64:215–20.
27. Awan AR, Chong YC, Field HJ. 1990. The pathogenesis of equine herpesvirus type 1 in the mouse: a new model for studying host responses to the infection. J Gen Virol 71:1131–40.
28. Awan AR, Baxi M, Field HJ. 1995. EHV-1-induced abortion in mice and its relationship to stage of gestation. Res Vet Sci 59:139–45.

29. Hasebe R, Kimura T, Nakamura K, Ochiai K, Okazaki K, Wada R, Umemura T. 2006. Differential susceptibility of equine and mouse brain microvascular endothelial cells to equine herpesvirus 1 infection. Arch Virol 151:775–86.

30. Nugent J, Birch-Machin I, Smith KC, Mumford JA, Swann Z, Newton JR, Bowden RJ, Allen GP, Davis-Poynter N. 2006. Analysis of Equid Herpesvirus 1 Strain Variation Reveals a Point Mutation of the DNA Polymerase Strongly Associated with Neuropathogenic versus Nonneuropathogenic Disease Outbreaks. J Virol 80:4047–60.

31. Niwa H, Yamamura K, Miyazaki J. 1991. Efficient selection for high-expression transfectants with a novel eukaryotic vector. Gene 108:193–9.

32. Szymczak AL, Workman CJ, Wang Y, Vignali KM, Dilioglou S, Vanin EF, Vignali DA. 2004. Correction of multi-gene deficiency in vivo using a single "self-cleaving" 2A peptide-based retroviral vector. Nat Biotechnol 22:589–94.

33. Schneider CA, Rasband WS, Eliceiri KW. 2012. NIH Image to ImageJ: 25 years of image analysis. Nat Methods 9:671–5.

34. David-Watine B, Israël A, Kourilsky P. 1990. The regulation and expression of MHC class I genes. Immunol Today 11:286–92.

35. Hartley WJ, Dixon RJ. 1979. An outbreak of Foal Perinatal Mortality due to Equid Herpesvirus Type I: Pathological Observations. Equine Vet J 11:215–8.

36. Whitwell KE, Blunden AS. 1992. Pathological findings in horses dying during an outbreak of the paralytic form of equid herpesvirus type 1(EHV-1) infection. Equine Vet J 24:13–9.

37. Smith PM, Zhang Y, Grafton WD, Jennings SR, O'Callaghan DJ. 2000. Severe murine lung immunopathology elicited by the pathogenic equine herpesvirus 1

strain RacL11 correlates with early production of macrophage inflammatory proteins 1alpha, 1beta, and 2 and tumor necrosis factor alpha. J Virol 74:10034–40.

38. Sakaguchi M, Watanabe M, Kinoshita R, Kaku H, Ueki H, Futami J, Murata H, Inoue Y, Li SA, Huang P, Putranto EW, Ruma IM, Nasu Y, Kumon H, Huh NH. 2014. Dramatic increase in expression of a transgene by insertion of promoters downstream of the cargo gene. Mol Biotechnol 56:621–30.

39. Whittemore SR, White LA. 1993. Target regulation of neuronal differentiation in a temperature-sensitive cell line derived from medullary raphe. Brain Res 615:27–40.

40. Wysocka J, Herr W. 2003. The herpes simplex virus VP16-induced complex: the makings of a regulatory switch. Trends Biochem Sci 28:294–304.

41. Ibrahim el SM, Pagmajav O, Yamaguchi T, Matsumura T, Fukushi H. 2004. Growth and virulence alterations of equine herpesvirus 1 by insertion of a green fluorescent protein gene in the intergenic region between ORFs 62 and 63. Microbiol Immunol 48:831–42.

42. Minato E, Aoshima K, Kobayashi A, Ohnishi N, Sasaki N, Kimura T. 2019. Exogenous Expression of Equine MHC Class I Molecules in Mice Increases Susceptibility to Equine Herpesvirus 1 Pulmonary Infection. Vet Pathol 56:703–10.

43. Livak KJ, Schmittgen TD. 2001. Analysis of relative gene expression data using real-time quantitative PCR and the 2-ΔΔCT method. Methods 25:402–8.

44. Kimura T, Okumura M, Kim E, Sasaki M, Orba Y, Sawa H. 2013. Characterization of Japanese encephalitis virus infection in an immortalized

mesencephalic cell line, CSM14.1. Microbiol Immunol 57:723–31.

45. Hudson SJ, Dix RD, Streilein JW. 1991. Induction of encephalitis in SJL mice by intranasal infection with herpes simplex virus type 1: A possible model of herpes simplex encephalitis in humans. J Infect Dis 163:720–7.

46. Drummond CW, Eglin RP, Esiri MM. 1994. Herpes simplex virus encephalitis in a mouse model: PCR evidence for CNS latency following acute infection. J Neurol Sci 127:159–63.

47. Kristie TM, Vogel JL, Sears AE. 1999. Nuclear localization of the C1 factor (host cell factor) in sensory neurons correlates with reactivation of herpes simplex virus from latency. Proc Natl Acad Sci USA 96:1229–33.

48. Wang IH, Burckhardt CJ, Yakimovich A, Greber UF. 2018. Imaging, tracking and computational analyses of virus entry and egress with the cytoskeleton. Viruses 10:1–29.

49. Pasdeloup D, Blondel D, Isidro AL, Rixon FJ. 2009. Herpesvirus Capsid Association with the Nuclear Pore Complex and Viral DNA Release Involve the Nucleoporin CAN/Nup214 and the Capsid Protein pUL25. J Virol 83:6610–23.

50. Patel J, Edington N. 1983. The pathogenicity in mice of respiratory, abortion and paresis isolates of equine herpesvirus-1. Vet Microbiol 8:301–5.

51. Nowotny N, Burtscher H, Bürki F. 1987. Neuropathogenicity for Suckling Mice of Equine Herpesvirus 1 from the Lipizzan Outbreak 1983 and of Selected other EHV 1 Strains. J Vet Med Ser B 34:441–8.

52. Bartels T, Steinbach F, Hahn G, Ludwig H, Borchers K. 1998. In situ study on the pathogenesis and immune reaction of equine herpesvirus type 1 (EHV-1) infections in mice. Immunology 93:329–34.

53. Walker C, Love DN, Whalley JM. 1999. Comparison of the pathogenesis of acute equine herpesvirus 1 (EHV-1) infection in the horse and the mouse model: A review. Vet Microbiol 68:3–13.

54. Gosztonyi G, Borchers K, Ludwig H. 2009. Pathogenesis of equine herpesvirus-1 infection in the mouse model. Apmis 117:10–21.

Summary in Japanese

ウマヘルペスウイルス 1 型（EHV-1）はヘルペスウイルス科 a ヘルペスウイルス亜科バリセロウイルス属に属する。EHV-1 は馬に呼吸器症状、流産および脊髄脳症を引き起こし、馬産業に経済的損失を与える。予防には生ワクチンあるいは不活化ワクチンが使用されているものの、日本を含む世界各地で EHV-1 感染症は発生している。

馬を用いた EHV-1 感染実験には施設的、費用的な制限がある。このことから、馬に代わる小動物モデルおよび *in vitro* モデルの開発が求められている。EHV-1 感染症の実験的感染ではマウスが用いられるが、マウスは脊髄脳症など EHV-1 感染症の重要な病態を再現しない。また、EHV-1 感受性の培養細胞モデルの数は限られており、EHV-1 感染に対する細胞種特異的な宿主の反応を解析することは困難である。特に、神経細胞が EHV-1 感染に抵抗性を示す機構は解明されていないが、これは神経細胞の *in vitro* モデルが存在しないためである。

EHV-1 感染症モデルの不足という課題を解決するため、本研究では、EHV-1 の機能的エントリーレセプターであるウマ主要組織適合遺伝子複合体（ウマ MHC class 1）遺伝子を導入することで、EHV-1 感受性のマウスモデルおよびラット由来神経細胞株モデルを作製した。第 1 章では、全身臓器にウマ MHC class 1 を発現するマウスを作製し、その EHV-1 感受性を検討した。作製した遺伝子導入マウス（Tg マウス）では、肺を含む様々な臓器でウマ MHC class 1 が発現していることが分かった。次に、Tg マウスおよび野生型の同腹仔（WT マウス）に EHV-1 を経鼻感染させた。この結果、WT マウスと比較して、Tg マウスの肺では、より多くの細胞が EHV-1 に感染していることが分か

った。以上の結果より、ウマ MHC class 1 を外来性に発現させることで、*in vivo* においてもマウス細胞の EHV-1 感受性を増強できることが明らかとなった。

第 2 章では、ラット由来神経細胞株 Rn33B にウマ MHC class 1 を遺伝子導入した細胞株 Rn33B-A68B2M を作製し、神経細胞における EHV-1 感受性を解析した。親株である Rn33B 細胞と同様に、Rn33B-A68B2M 細胞は 32℃での培養で未分化状態を維持し、37℃での培養で神経様に分化した。神経病原性株である EHV-1 Ab4 を用いた感染実験により、未分化細胞では EHV-1 増殖が認められるのに対し、分化細胞ではこれが抑制されることが分かった。興味深いことに、HSV-1 を Rn33B 細胞に感染させた場合、細胞の分化状態に関わらずウイルス増殖が認められた。これらの結果から、Rn33B-A68B2M 細胞は分化依存性に EHV-1 抵抗性を獲得することが示唆された。

本研究により、*in vivo* で発現したウマ MHC class 1 が EHV-1 感染 Tg マウスにおける肺病変の形成に影響することが明らかとなった。また本研究では、ラット由来神経細胞株を用いた *in vitro* モデルを作製し、同モデルは分化依存性の EHV-1 抵抗性を示した。これらのモデルは EHV-1 感染症における分子学的病理機構の解明に貢献するものと期待される。